

**DENOISING OF COVID-19 CT IMAGE USING A NOVEL  
ADAPTIVE WEIGHTED MEDIAN FILTER WITH  
META-HEURISTIC ALGORITHM**

*A Project report submitted in partial fulfillment of the requirements for  
the award of the degree of*

**BACHELOR OF TECHNOLOGY  
IN  
ELECTRONICS AND COMMUNICATION ENGINEERING**

*Submitted by*

**P. Pallavi (319126512045)**

**B. Jaya Kishor (319126512006)**

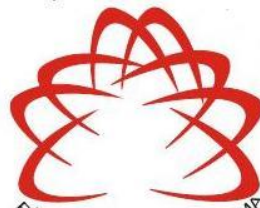
**G. Chakradhar Naidu (319126512017)**

**B.S. Sai Preetham (319126512009)**

**Under the guidance of**

**Mr. Bibekananda Jena – B. Tech, M. Tech, (Ph.D.)**

**Assistant Professor**



**ANITS**

**DEPARTMENT OF ELECTRONICS AND COMMUNICATION  
ENGINEERING**

**ANIL NEERUKONDA INSTITUTE OF TECHNOLOGY AND SCIENCES  
(UGC AUTONOMOUS)**

*(Permanently Affiliated to AU, Approved by AICTE and Accredited by NBA & NAAC )  
Sangivalasa, bheemili mandal, visakhapatnam dist.(A.P)*

**2022-2023**

DEPARTMENT OF ELECTRONICS AND COMMUNICATION  
ENGINEERING  
ANIL NEERUKONDA INSTITUTE OF TECHNOLOGY AND SCIENCES  
(UGC AUTONOMOUS)  
(Permanently Affiliated to AU, Approved by AICTE and Accredited by NBA &  
NAAC)  
Sangivalasa, Bheemili mandal, Visakhapatnam dist. (A.P)



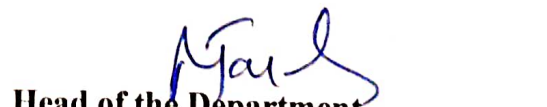
CERTIFICATE

*This is to certify that the project report entitled "Denoising of COVID-19 CT image using a novel adaptive weighted median filter with meta-heuristic algorithm" submitted by P. Pallavi (319126512045), B. Jaya Kishor (319126512006), G. Chakradhar Naidu (319126512017), B.S. Sai Preetham (319126512009) in partial fulfillment of the requirements for the award of the degree of Bachelor of Technology in Electronics & Communication Engineering of Anil Neerukonda Institute of technology and Sciences(A), Visakhapatnam is a record of bonafide work carried out under my guidance and supervision.*



**Project Guide**  
**Mr. B. Jena**  
B. Tech, M. Tech, (Ph.D)  
Asst. Professor  
Department of E.C.E  
ANITS  
Assistant Professor  
Department of E.C.E.  
Anil Neerukonda

Institute of Technology & Sciences  
Sangivalasa, Visakhapatnam-531 162



**Head of the Department**  
**Dr. B. Jagadeesh**  
B.E.,M.E.,Ph.D.,FIE,FIETE,MIEEE  
Professor & HOD  
Department of E.C.E  
ANITS

**Head of the Department**  
Department of E C E  
Anil Neerukonda Institute of Technology & Science  
Sangivalasa - 531 162

## **ACKNOWLEDGEMENT**

We would like to express our deep gratitude to our project guide **Mr. B. Jena**, Asst. Professor, Department of Electronics and Communication Engineering, ANITS, for his guidance with unsurpassed knowledge and immense encouragement. We are grateful to **Dr. B. Jagadeesh**, Head of the Department, Electronics and Communication Engineering, for providing us with the required facilities for the completion of the project work.

We are very much thankful to the **Principal and Management, ANITS, Sangivalasa**, for their encouragement and cooperation to carry out this work.

We express our thanks to all **teaching faculty** of Department of ECE, whose suggestions during reviews helped us in accomplishment of our project. We would like to thank **all non-teaching staff** of the Department of ECE, ANITS for providing great assistance in accomplishment of our project.

We would like to thank our parents, friends, and classmates for their encouragement throughout our project period. At last, but not the least, we thank everyone for supporting us directly or indirectly in completing this project successfully.

### **PROJECT STUDENTS**

P. Pallavi (31912612045)

B. Jaya Kishor (319126512006)

G. Chakradhar Naidu (319126512017)

B.S. Sai Preetham (319126512009)

## **ABSTRACT**

When COVID-19 was still in its early phases, the only technology for detecting the SARS-COV-2 virus was nucleic acid detection (RT-PCR). However even after being a highly reliable technique it's accuracy in terms of detecting COVID-19 was low. It was then that CT scan was put into practice for detection. However, owing to its radiation effects CT scan was performed with low dose. The problem due to low dose is CT image being susceptible to noise both during start (transmission) and end (acquisition) of process. CT scans for various stages of SARS-COV-2 detection posed different problems like: low density image of early stage making it not so difficult to confuse with noise, features like lesions being not detected properly with reason being low contrast and so, no proper distinction between different phases of COVID-19. So here we are making use of a novel adaptive weighted median filtering method based on meta heuristic algorithm in an attempt to denoise the image. So as to get a clear CT image (aiming at the problems mentioned) for the medical team to be able to analyze and fetch information from it with ease. Peak signal-to-noise ratio (PSNR), mean square error (MSE), and image enhancement factor (IEF) of the image are used in the results to demonstrate the improvement



# CONTENTS

<b>LIST OF SYMBOLS</b> .....	<b>vi</b>
<b>LIST OF FIGURES</b> .....	<b>viii</b>
<b>LIST OF TABLES</b> .....	<b>x</b>
<b>LIST OF ABBREVIATIONS</b> .....	<b>x</b>
<b>1. INTRODUCTION</b> .....	<b>1</b>
1.1 Overview .....	1
1.1.1 RT-PCR .....	1
1.1.2 Working of RT-PCR for COVID-19 detection .....	1
1.1.3 CT scan.....	2
1.1.4 CT scan Working.....	3
1.1.5 Magnetic Resonance Imaging (MRI) .....	4
1.1.6 Applications of MRI.....	4
1.1.7 CT Scan Vs MRI .....	5
1.2 Motivation .....	6
1.3 Objective of the thesis .....	6
1.4 Organisation of the thesis .....	7
1.5 Image processing for medical images .....	7
<b>2. LITERATURE SURVEY</b> .....	<b>8</b>
<b>3. IMAGE PROCESSING PRELIMINARIES</b> .....	<b>9</b>
3.1 Introduction to Digital Image Processing.....	9
3.2 Purpose of Digital Image Processing .....	10
3.3 Analog and Digital Image Processing .....	10
3.3.1 Analog Image Processing .....	10
3.3.2 Digital Image Processing.....	11
3.3.1 Analog Vs Digital Image Processing .....	11
3.4 Types of Images .....	12
3.5 Noise and its Types .....	14
3.6 Digital Image Processing techniques .....	15
3.7 Applications.....	18
<b>4. SPATIAL DOMAIN DENOISING APPROACH</b> .....	<b>20</b>
4.1 Spatial Domain Processing.....	20
4.2 Spatial Filters.....	21

4.3 Mean Filter .....	23
4.4 Adaptive Weighted Mean Filter .....	24
4.5 Median Filter .....	24
4.6 Adaptive Weighted Median Filter .....	25
4.7 Non-Local Mean Filter .....	25
<b>5. METHODOLOGY .....</b>	<b>27</b>
5.1 Introduction .....	27
5.2 Adaptive Multi-level Thresholding .....	28
5.2.1 Methodology.....	29
5.3 Meta heuristic Optimization Algorithm .....	31
5.4 Aquila Optimizer.....	32
5.4.1 Methodology.....	33
5.5 Arithmetic Optimization Algorithm.....	39
5.5.1 Methodology.....	40
5.6 Center Weighted Median Filter .....	44
5.6.1 Methodology.....	45
<b>6. RESULTS AND DISCUSSIONS .....</b>	<b>48</b>
6.1 Introduction .....	48
6.2 Image Quality Metrics.....	48
6.2.1 PSNR .....	49
6.2.2 MSE.....	50
6.2.3 IEF .....	51
6.3 Simulated Parameter Values .....	52
6.4 Resultant CT Images .....	54
6.4.1 Filtered Images using Aquila Optimizer .....	54
6.4.2 Filtered Images using Arithmetic Optimizer .....	59
6.5 Result Analysis.....	65
<b>7. CONCLUSION AND FUTURE WORK .....</b>	<b>66</b>
<b>REFERENCES.....</b>	<b>67</b>
<b>PUBLISHED PAPER .....</b>	<b>69</b>

## LIST OF SYMBOLS

$'TH_0'$	First threshold value
$\overline{M}_U'$	Average gray value of all pixels in top neighbourhood of filter window
$\overline{M}_D'$	Average gray value of all pixels in bottom neighbourhood of filter window
$\overline{M}_L'$	Average gray value of all pixels in left neighbourhood of filter window
$\overline{M}_R'$	Average gray value of all pixels in right neighbourhood of filter window
$'g_{med}'$	Median gray value of all the pixels in filter window
$'g_{ave}'$	Average gray value of all the pixels in filter window
$'g(i,j)'$	Gray value of pixel at position (i,j)
$\overline{g}_{min}'$	Adaptive minimum value
$\overline{g}_{max}'$	Adaptive maximum value
$'n \times n'$	Size of the filter window
$'TH_1'$	Second threshold value
$'\varphi'$	Regulatory factor of $TH_1$
$'p'$	Noise density
$'N_{pn}'$	No. of noise pixels in filter window
$'t'$	Current iteration for AO algorithm
$'T'$	Maximum iterations for AO algorithm
$'P=[p_{1,1}, p_{1,2}, \dots, p_{N,Dim}]'$	Set of parameters for AO algorithm
$'P_{best}(t)'$	Best parameter value obtained till $t^{th}$ iteration
$'P_M(t)'$	Mean value of the parameters at $t^{th}$ iteration
$'Levy(D)'$	Levy flight distribution function

<i>'Dim'</i>	Dimension size
<i>'N'</i>	Population size
<i>'UB'</i>	Upper boundary
<i>'LB'</i>	Lower boundary
<i>'QF'</i>	Quality function
<i>'S=[s<sub>1,1</sub>, s<sub>1,2</sub>, ..., s<sub>N,n</sub>]</i>	Set of parameters for AOA algorithm
<i>'C_Iter'</i>	Current iteration for AOA algorithm
<i>'M_Iter'</i>	Maximum iterations for AOA algorithm
<i>'MOA(C_Iter)'</i>	Math Optimizer Accelerated function
<i>'MOP(C_Iter)'</i>	Math Optimizer Probability
<i>'μ'</i>	Parameter to adjust search process in AOA
<i>'γ<sub>1</sub>(i, j)'</i> and <i>'γ<sub>2</sub>(i, j)'</i>	Weighted sub coefficients
<i>'γ(i, j)'</i>	Weighted coefficient
<i>'η<sub>1</sub>'</i> and <i>'η<sub>2</sub>'</i>	Optimization parameters
<i>'g(i, j)<sub>CWM</sub>'</i>	Center Weighted Median

## LIST OF FIGURES

<b>Figure no.</b>	<b>Title</b>	<b>Page no.</b>
Fig. 1.1	CT machine	3
Fig. 1.2	MRI scan machine	4
Fig. 3.1	Digital Image Processing System	9
Fig. 3.2	Binary image of sea creatures	12
Fig. 3.3	RGB image converted to its grayscale version	13
Fig. 3.4	Splitting of an image into its Red, Green and Blue channels	13
Fig. 3.5	Example of changing the ‘alpha’ parameter in RGBA images	14
Fig. 3.6	Types of noise	14
Fig. 3.7	Example of Image restoration	16
Fig. 3.8	Example of Image manipulation	17
Fig. 3.9	Example of Image-to-Image translation	17
Fig 3.10	Hurdle detection robot and Line follower robot	18
Fig. 4.1	Illustration of Spatial Domain	20
Fig. 4.2	Spatial domain for color image (RGB)	21
Fig. 4.3	Filtering in spatial domain	22
Fig. 4.4	3×3 Mean Filtering	23
Fig. 4.5	Median Filtering	25
Fig. 5.1	Flowchart of the process in brief	27
Fig. 5.2	Flowchart of Adaptive multi-level thresholding	28
Fig. 5.3	Representation of filter window of size 5×5	30
Fig. 5.4	The behaviour of the Aquila high soar with vertical stoop	34
Fig. 5.5	The behaviour of the Aquila contour flight with short glide attack	35
Fig. 5.6	The behaviour of the Aquila low flight with slow descent attack	36
Fig. 5.7	The behaviour of the Aquila walks and grab prey	37
Fig. 5.8	Flowchart of AO technique	39
Fig. 5.9	Hierarchy of Arithmetic operators	40
Fig. 5.10	Model of updating the position of math operators in AOA toward the optimum area	43
Fig. 5.11	Flowchart representing the process flow of AOA algorithm	44
Fig. 5.12	Flowchart depicting the complete process	47

Fig. 6.1	Results of CT image of early COVID-19 using AO	54
Fig. 6.2	Results of CT image of advanced COVID-19 using AO	55
Fig. 6.3	Results of CT image of early COVID-19 with non-symptom using AO	56
Fig. 6.4	Results of CT image of advanced COVID-19 with non-symptom using AO	57
Fig. 6.5	Results of CT image of adenovirus pneumonia using AO	58
Fig. 6.6	Results of CT image of early COVID-19 using AOA	59
Fig. 6.7	Results of CT image of advanced COVID-19 using AOA	60
Fig. 6.8	Results of CT image of early COVID-19 with non-symptom using AOA	61
Fig. 6.9	Results of CT image of advanced COVID-19 with non-symptom using AOA	62
Fig. 6.10	Results of CT image of adenovirus pneumonia using AOA	63
Fig. 6.11	Comparison of PSNR for CT scans with varying noise densities for different filtering techniques	64

## LIST OF TABLES

<b>Table no.</b>	<b>Title</b>	<b>Page no.</b>
Table 1.1	Differences between CT scan and MRI	<b>5</b>
Table 3.1	Comparison between analog and digital image processing	<b>11</b>
Table 6.1	Results of different phases of COVID-19 using AO	<b>52</b>
Table 6.2	Results of different phases of COVID-19 using AOA	<b>53</b>

## LIST OF ABBREVIATIONS

RT-PCR	Reverse transcriptase-polymerase chain reaction
DNA	Deoxyribonucleic acid
CT	Computed Tomography
MRI	Magnetic Resonance Imaging
MSE	Mean Square Error
PSNR	Peak Signal-to-Noise Ratio
IEF	Image Enhancement Factor
COVID-19	Coronavirus disease (2019)
SARS-COV-2	Severe Accurate Respiratory Syndrome Coronavirus 2
3D	3 Dimensional
2D	2 Dimensional
AO	Aquila Optimizer
AOA	Arithmetic Optimization Algorithm
CWM	Center Weighted Median

# **CHAPTER I**

## **INTRODUCTION**

### **1.1 Overview**

COVID-19 has become widely circulating from December 2019 all over the world. People with weak immune systems are most seriously affected by COVID-19, and children and pregnant women are particularly vulnerable. The main problem is identifying COVID-19 using several tests such as chest CT and RTPCR (polymerase chain reaction). The RTPCR is relatively poor and not sensitive enough for diagnostic procedure with a potential for giving misleading results. Hence, CT is crucial in the diagnosis of COVID-19. In order to provide digital medical imaging of the human body, computed tomography (CT) is utilized in medical applications. CT imaging is acquired through the reconstruction process, with X-rays serving as its primary imaging source. New research areas in technology and medical devices have emerged as a result of the current coronavirus outbreak.

#### **1.1.1 RT-PCR**

Real-time reverse transcription-polymerase chain reaction (real-time RT-PCR), one of the quickest and most precise laboratory techniques for detecting, following, and researching the COVID-19 virus, is being used by some nations with the assistance of the IAEA and the Food and Agriculture Organization of the United Nations (FAO).

#### **1.1.2 Working of RT-PCR for COVID-19 detection**

A sample is obtained from the nose and throat since the COVID-19 virus prefers to gather in those parts of the body. Following a series of chemical processes, the sample's RNA is separated from other substances like proteins and lipids. This retrieved RNA



contains the virus, if any, together with the individual's own genetic material. Reverse transcription of the RNA into DNA is carried out by a specific enzyme. Then, researchers add additional short DNA fragments that complement specific parts of the transcribed viral DNA. If the virus is present in the sample, these fragments bind to specific areas of the viral DNA. During amplification, some of the extra genetic information is used to make DNA strands, while others are not.

The mixture is then put inside the RT-PCR device. In order to initiate precise chemical reactions that duplicate the targeted viral DNA segments in new, identical copies, the gadget alternately heats and cools the liquid. The cycle is continually repeated to maintain replication of the viral DNA sections targeted. Each cycle doubles the preceding number, thus two copies become four, four copies become eight, and so on. Each strand of the virus present in the sample has generated around 35 billion more copies of the viral DNA segments by the time a standard real-time RT-PCR system has finished 35 cycles.

As new copies of the viral DNA sections are made, the marker labels bond to the DNA strands and release fluorescent dye that is tracked by the machine's computer and shown in real time on the screen. The computer records the fluorescence levels of the sample after each cycle. When fluorescence rises above a particular level, the virus is present. Researchers also track the number of cycles necessary to attain this level in order to determine the severity of the infection. The severity of the viral infection increases with decreased cycle requirements.

### **1.1.3 CT Scan**

The imaging process known as computed tomography (CT) employs specialised x-ray equipment to produce in-depth images, or scans, of various bodily regions. It is also known as computerised axial tomography and computerised tomography. (CAT). A narrow x-ray beam is quickly spun around a patient's body during a procedure known as "computed tomography," or CT. This produces signals that are then analysed by the machine's computer to create cross-sectional images, or "slices," of the patient's body. These sections, which are known as tomographic pictures, can provide a clinician with

more specific information than traditional x-rays. Once the slices have been gathered, the machine's computer may digitally "stack" a number of subsequent slices to produce a three-dimensional (3D) image of the patient.

#### **1.1.4 CT Scan Working**

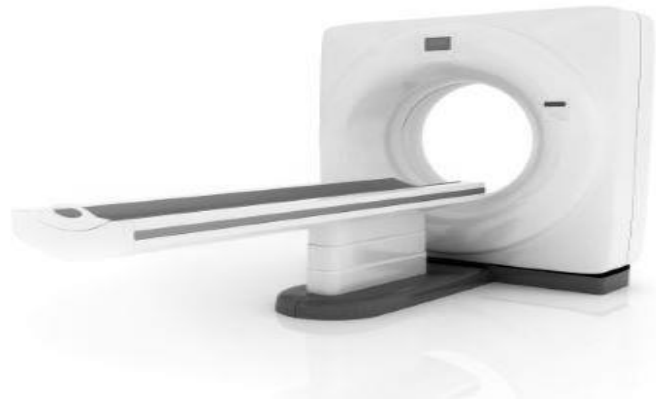


Figure 1.1 A CT machine

Unlike a standard x-ray, which uses a stationary x-ray tube, a CT scanner uses a motorised x-ray source that spins through a circular entrance of a donut-shaped frame called a gantry. In a CT scan, a patient lies on an inflatable mattress that slowly rotates over the gantry while an x-ray tube fires a narrow beam of radiation into their body. Instead of using film, CT scanners employ specialised digitalized x-ray detectors that are positioned directly across from the x-ray source. The x-rays are captured by the imaging devices as they leave the patient and are then sent to a computer.

Every time the x-ray source completes a full rotation, the CT computer creates a two-dimensional imaging slice of the patient using sophisticated mathematical techniques. The size of the tissue visible in each imaging slice may vary depending on the CT system being used, although it normally ranges from 1 to 10 cm. The image is saved after completing a full slice, and the motorised bed is then gradually lowered onto the gantry. The x-ray scanning process is then repeated to create a new image slice. Up until the necessary amount of slices have been acquired, this process is repeated.

The computer has the option of displaying the image slices one at a time or stacking them to build a three-dimensional image of the patient's body that shows the bones,

organs, tissues, and any anomalies the doctor is expecting to find. The ability to view slices sequentially or to reorient the three-dimensional image in space are two advantages of this method that make it easier to identify the specific position of a potential problem.

### **1.1.5 Magnetic Resonance Imaging (MRI)**



Figure 1.4 MRI scan machine

A non-invasive imaging technique called the magnetic resonance imaging (MRI) creates three-dimensional, intricate anatomical images. Similar to CT scans, it is one among the most popular scans. For illness identification, diagnosis, and therapy monitoring, it is frequently employed. Based on cutting-edge technology, it stimulates and detects changes in the axis of rotation of protons in the fluid that makes up tissues that are alive

### **1.1.6 Applications of MRI**

MRI scanners are especially well adapted for imaging the body's soft tissues or non-bony portions. They are distinct from computed tomography (CT) in that they do not utilise x-rays' harmful ionising radiation. Because MRI provides a far clearer view of the brain, spinal cord, and nerves than conventional x-rays and computed tomography (CT), it is frequently used to assess knee and shoulder injuries. Aneurysms and tumours can also be identified with MRI, which can also distinguish between white matter and grey matter in the brain. When frequent imaging is needed for diagnosis or therapy, particularly in the brain, MRI is the imaging modality of choice because it does not use

x-rays or other radiation. But MRI is more expensive than CT scanning or x-ray imaging.

Functional Magnetic Resonance Imaging is one type of specialised MRI. (fMRI.) This is done to look at brain architecture and see which parts of the brain "activate" (use more oxygen) when performing different kinds of cognitive tasks. It presents a potential new standard for evaluating neurological health and risk for neurosurgery and is utilised to increase our understanding of how the brain is organised.

### 1.1.7 CT SCAN Vs MRI

Table 1.1 Differences between CT scan and MRI

	<b>CT Scan</b>	<b>MRI</b>
<b>Principle</b>	combines several X-rays obtained at various angles to create cross-sectional images.	produces detailed images using strong magnetic fields and radio frequency pulses.
<b>Radiation</b>	Minimal	None
<b>Uses</b>	Excellent for viewing soft tissue and extremely good for observing bone, especially when used in conjunction with intravenous contrast dye	highly good at seeing minute variations in soft tissue
<b>Cost</b>	typically, more affordable than an MRI	Frequently more costly than CT scans
<b>Time taken</b>	Depending on the size of the region being scanned, it only takes approximately 5 minutes.	depends on the body part being investigated and might last anywhere between 15 minutes and two hours.
<b>Application</b>	creates a broad impression of a region, such as internal organs, fractures, or head injuries	produces more precise images of organs, ligaments, and soft tissue
<b>Benefits</b>	quicker and can provide images of the skeletal structure, tissue, and organs	creates images with greater detail
<b>Risks</b>	<ul style="list-style-type: none"> <li>• • Negative for unborn children</li> <li>• • A very low radiation dosage</li> <li>• • A possible adverse effect from the use of dyes</li> </ul>	<ul style="list-style-type: none"> <li>• • Magnets may cause a reaction with metals</li> <li>• • Hearing problems may result from the machine's loud noises.</li> <li>• • Body temperature rising during prolonged MRIs</li> <li>• • Claustrophobia</li> </ul>

## **1.2 Motivation:**

In the beginning, the most popular technique for identifying COVID-19 was nucleic acid testing. (RT-PCR). However, RT-PCR screening suffers from a low sensitivity issue. The suspected patient may still have SARS-Cov-2 infection even if the RT-PCR test results are negative. Nucleic acid testing also has the drawback of taking a long time and requiring specialised test kits. The CT scan method—which was quicker and more effective in terms of COVID detection—was chosen in order to increase the detection speed and decrease the cost. Nevertheless, impulsive noise during transmission and acquisition compromised the COVID-19 CT image. Patients will be exposed to high levels of radiation during CT scans, which is extremely damaging to their health. Because of this, decreasing the CT dose at this time usually lessens the harm to the patient's health. However, noise is frequently visible in CT images taken at modest doses. Noise production will affect CT scan quality, which will significantly affect the doctor's ability to determine the patient's ailment.

## **1.3 Objective of the thesis:**

In contrast to currently popular techniques, the goal of this thesis is to provide a novel medical picture denoising methodology that focuses on the creation of high-performance algorithms. The many noises used in the acquisition, transmission, and storage of lung computed tomography (CT) images introduce random, discrete, and isolated pixels into the image. The ability to segment lesions and the ability of clinicians to evaluate patients' conditions are both negatively impacted by this picture noise. Here we used a novel adaptive weighted median filter with a meta-heuristic algorithm to denoise the CT image which will be discussed later.

## **1.4 Organisation of the thesis**

There are 8 chapters in the entire report, the first one is all about the objective of our project along with some introduction. Second chapter is about the papers considered and a little information about each of the (literature survey). Third chapter explains the preliminaries of Digital Image Processing. The next chapter is all about various filters that are used for removal of different types of noise. Fifth chapter gives out the

implementation part of the project explaining the blocks we considered, their working and so. Sixth chapter is all about the results simulated explained using various parameters and images. Seventh chapter concludes the report and this followed by references in the next chapter.

## **1.5 Image processing for medical images**

Segmentation and texture analysis are two methods used in the detection of cancer and other diseases. In particular, the more recent PET-CT and PET-MRI modalities frequently use contemporary imaging techniques including image fusion and registration. The area of bioinformatics uses telemedicine and format-less compression techniques to send images over great distances.

Edge detection, pattern matching, denoising, security, and biometric techniques such as identification, face, and fingerprint documentation are frequently utilized in this industry. The information in the databases about the people is the foundation of forensics. To establish a person's identity, forensics compares the input data (fingerprint, eye, photo, etc.) with the database.

## **CHAPTER II**

### **LITERATURE SURVEY**

In the early phase of COVID-19 pandemic era, RT-PCR test was the only method available to carry out the SARS-COV-2. It was done by considering the samples of throat and sputum out of which sputum samples showed high positive rates than the throat samples [1]. Though this test is considered as golden standard for nucleic acid tests due to its high sensitivity and reliability, there were some concerns regarding its accuracy. As not all the patients infected with SARS-COV-2 showed positive result when tested for the same using RT-PCR. Additionally with the exponential rise in cases this test alone was not enough for the masses considering its testing time and low availability of the kits. This issue then demanded for the test of clinical features through CT scan [2,3]. When tested for its consistency, CT scan was found to be more effective than RT-PCR in terms of both detection speed and sensitivity [4]. The ability to recognize these persons is aided by a few characteristics shown in the CT scans of SARS-COV-2 patients, such as ground-glass opacities, pulmonary sclerosis, interlobular septal thickening, pulmonary fibrosis, and many lesions. [6-7]. However, CT scans taken with high dose pose the risk of cancer, considering which low CT doses are used for COVID-19 detection by changing certain parameters of CT scanning [8]. However, usage of low dose for these purposes comes with the disadvantage of noise addition to these CT images. Here, in this project we're trying to eliminate salt and pepper noise (impulse noise). [9] Outlines usage of methods like adaptive multi-level thresholding, Optimized weighted median filter for the purpose of image denoising. A key block in our denoising approach would be the optimization techniques we used here i.e., Aquila and Arithmetic optimization techniques. These techniques are used to find the weighted parameters [10-11]. Some of the filters used for denoising different noise, including sudden noise For instance, a salt and pepper sound of different densities are mentioned here [12-16]

# CHAPTER III

## IMAGE PROCESSING PRELIMINARIES

### 3.1 Introduction to Digital Image Processing

The process of modifying digital photos using a computer is termed as digital image processing. It is a specialized field of systems and signals with a significant focus on images. DIP's main objective is to establish a system of computers that can do processing images. Algorithms are employed in digital image processing to alter pictures. Photoshop by Adobe is the most frequently utilized programs for processing digital pictures.

**For example:** Adobe Photoshop, MATLAB, etc.

It additionally serves for transforming image data from sensors into digital images. Image processing make use of an array of algorithms.



Figure 3.1 Digital Image Processing system



## **3.2 Purpose of Digital Image Processing**

Images are enhanced for easier understanding by people. Images may be analyzed and data retrieved for automated interpretation. By modifying the image's pixels, you may obtain whatever you want in density and contrast. Images may be readily retained and retrieved.

The primary goal of the image processing process is to convert an image in digital form and then conduct particular operations within it in order to generate specified models or extract relevant information from the picture.

Some of the common purposes for which image processing is used are:

- **Visualizing:** This entails manipulating photos that have been captured with a camera to try to enhance them or achieve more favourable outcomes. This could involve zooming, upscaling, blurring, sharpening, transforming between grayscale to colors, locating edges, extracting images, and detecting images.
- **Image sharpening and restoration:** This mainly involves improving noisy photos.
- **Image retrieval:** High-resolution image search has been referred to here.
- **Pattern recognition:** This involves defining several image parts.
- **Image recognition:** Recognizing objects in the image is needed for this.

## **3.3 Analog and Digital Image processing**

### **3.3.1 Analog Image Processing**

Only two-dimensional signals are handled by analog image processing, it is applied to analog signals. Electrical impulses are used for changing the visuals. Signals that are analog can be regular or non-periodic in analogue image processing.

**Examples** Television images, pictures, art, and medical images are instances of analog images.

### 3.3.2 Digital Image Processing

Digital pictures undergo to photographic processing. (a matrix of small pixels and elements). A wide range of tools and methods are used for performing modifications on pictures when they are manipulated. Digital image processing is one of today's quickest expanding sectors, and it has an impact on everyone's lives.

**Examples** are Color processing, recognition of images, video processing, and additional digital image processing techniques.

### 3.3.3 Analog Vs. Digital Image Processing

The following differences exist between Analog Processing of Images and Digital Picture Processing:

<b>Analog Image Processing</b>	<b>Digital Image Processing</b>
Analog processing images is used on analog signals and only utilizes two-dimensional signals.	Digital processing of images refers to generate electrical signals that carry out on image evaluation and manipulation.
Because analog signals shift over time, the pictures generated through analog image processing change.	It increases the digital level of the image and has suitable intensity distribution.
Analog processing of images is a more laborious and costly procedure.	Digital photo processing is a more inexpensive and faster way of keeping and retrieving images.

The analog feed is real-world, but the image quality is poor.	It employs efficient picture algorithms for compression to lower the quantity of data necessary while generating photographs of high quality.
It is usually continuous and not separated into tiny pieces.	It utilizes an image segmentation look at to detect discontinuity resulting from an impaired relating path.

Table 3.1 Comparison between Analog and Digital image processing

### 3.4 Types of Images

#### 1. Binary Image

Binary images include just two unique pixel intensity values: 0 (which symbolize black) and 1 (which represents white). These graphic elements are usually employed to emphasise a distinguishing part in a coloured image. For example, as seen below, it is frequently employed for image segmentation.

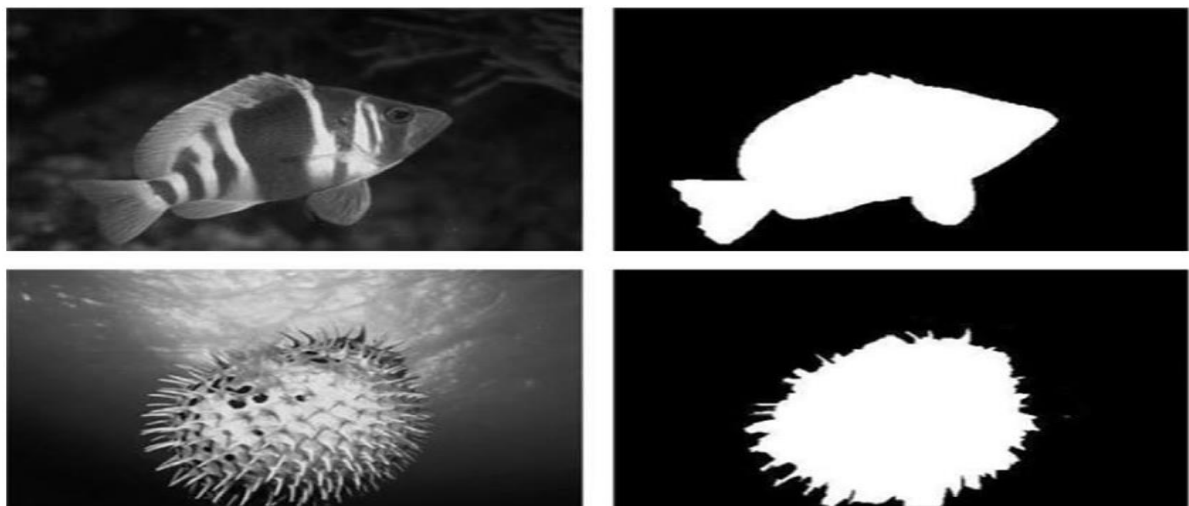


Figure 3.2 Binary image of sea creatures

## 2. Grayscale Image

Grayscale or 8-bit pictures are formed up of 256 different colors, with the intensity of each pixel from 0 to 255 indicating black and white, accordingly. The remaining 254 values are different colors of gray.

The image below is an instance of an RGB picture translated to grayscale. The shape of the distribution remains constant for both the RGB and gray scale photos.

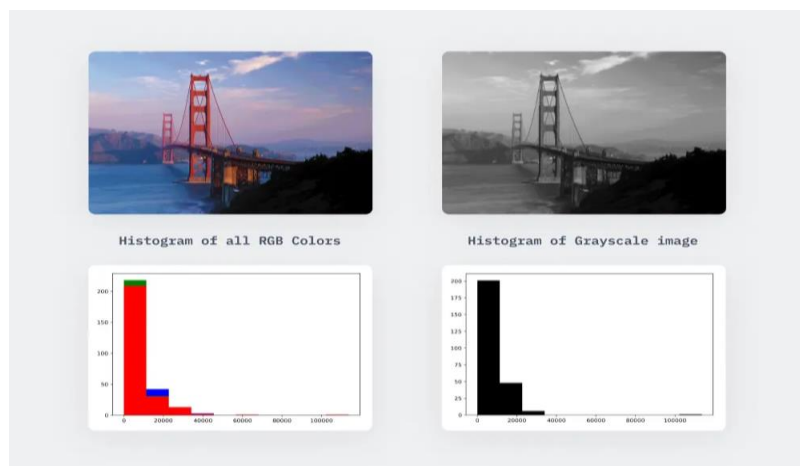


Figure 3.3 RGB image converted to its grayscale version

## 3. RGB Color Image

In nowadays, we are used to observing RGB or coloured images, which are 16-bit matrix to computers. That implies each pixel could contain up to 65,536 distinct colours. "RGB" refers to an image's red, green, and blue "channels."

Below is a representation of an RGB image divided into its channel components. The structures of the histograms for all of those channels are distinct.

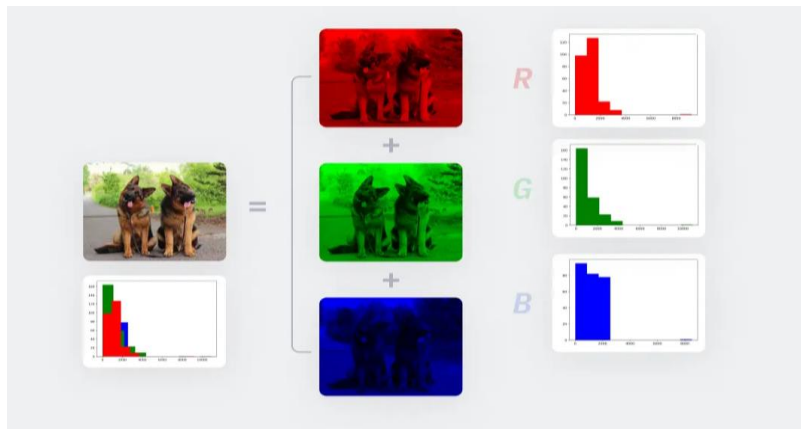


Figure 3.4 Splitting of an image into its Red, Green and Blue channels

#### 4. RGBA Image

RGBA pictures consist of color RGB images with another channel called "alpha" that represents the transparency of the RGB image. Opacity has a value that ranges from 0% to 100% and is efficiently a "see-through" characteristic.

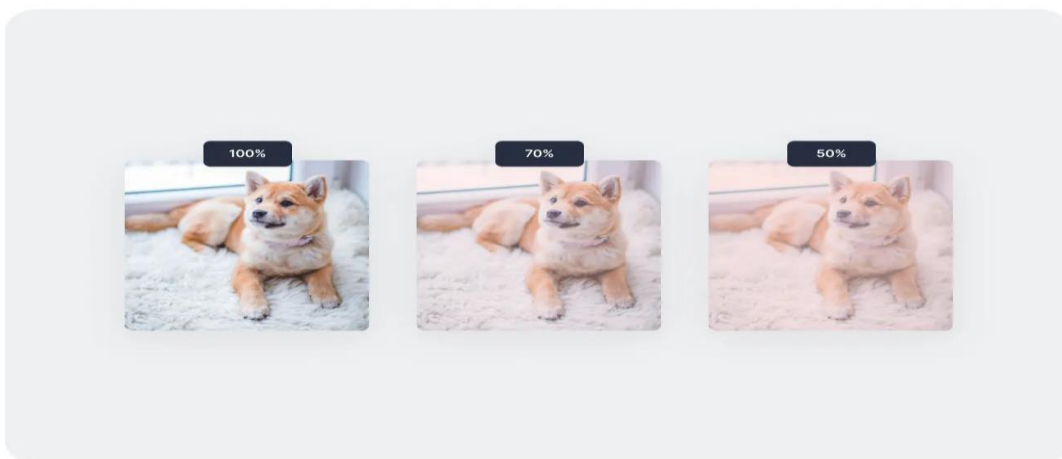


Figure 3.5 Example of changing the “alpha” parameter in RGBA images

### 3.5 Noise and its Types

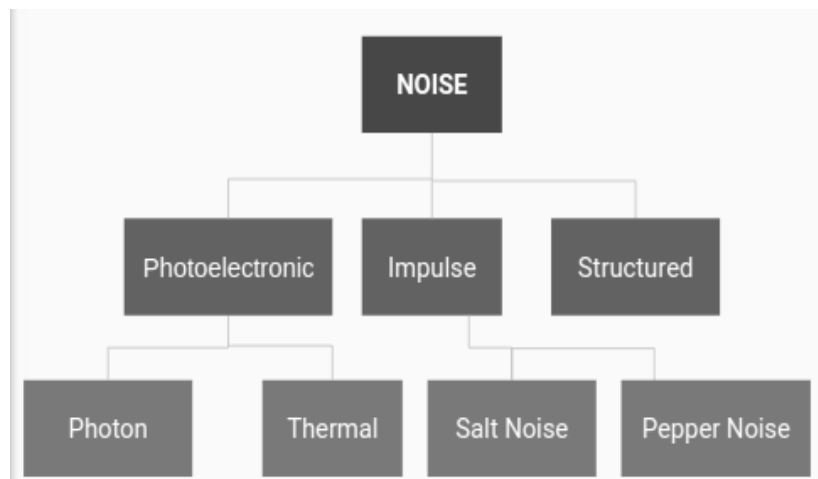


Figure 3.6 Types of noises

#### 1. Gaussian Noise

Gaussian Noise, also known as Gaussian Distribution, is a statistical noise with a density function whose probability is equal to the normal distribution. In order to generate this noise, a random Gaussian function is added to the Image function. Because it takes place in amplifiers or detectors, it can be referred to as electronic noise.

#### 2. Impulse Noise

There are three categories of impulse noises. Salt Noise, Pepper Noise, Salt and Pepper Noise.

- **Salt Noise:** Salt noise is produced by spreading random bright (255-pixel) pixels across a picture.
- **Pepper Noise:** Salt noise is generated by scattering a random black (with a pixel value of 0) over a picture.
- **Salt and Pepper Noise:** Noise composed of salt and pepper can be added to an image by spreading both random bright (255-pixel value) or random dark (0-

pixel value) pixels over the image. Because it statistically drops the initial information values, this kind of model is referred to as data drop noise.

### **3. Poisson Noise**

The statistical character of electromagnetic radiation such as x-rays, visible lights, and gamma rays causes the appearance of this noise.

This kind of noise can be referred to as quantum (photon) noise and shot noise.

### **4. Speckle Noise**

The occurrence of speckle noise in the picture reconstruction process is an important hurdle in optical and digital holography. Speckle is granular noise that appears essentially in images and reduces their quality. Speckle noise may be created by dividing random pixel values across multiple picture pixels.

## **3.6 Digital Image processing techniques**

There are 8 image processing techniques which are mentioned below:

1. ***Image enhancement:*** picture enhancement, or expanding the level of detail of a photo, is one of the most usual image processing operations. It is helpful for machine vision responsibilities, positioning, and monitoring. Adjusting an image's brightness and contrast is a typical planning.
2. ***Image restoration:*** Image quality can decrease for a variety of reasons, particularly photographs taken before cloud storage was widely available. Images transferred from hard copies shot with vintage instant cameras, for example, frequently get scratches.

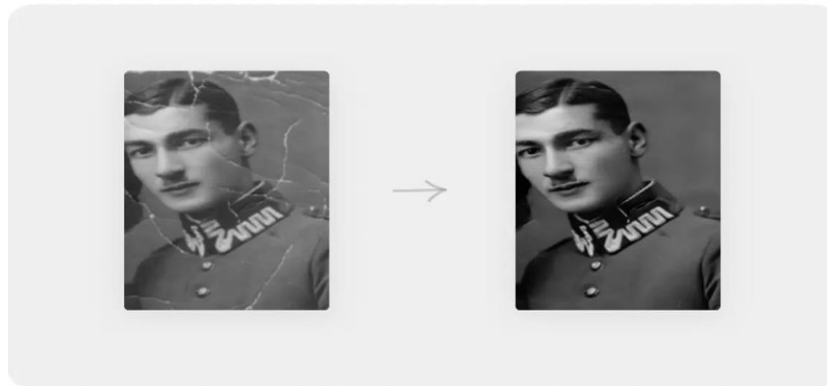


Figure 3.7 Example of Image restoration

3. **Image segmentation:** The technique of splitting one picture into numerous parts or areas is known as image segmentation. The segmentation of images is often used as an initial processing stage for object recognition since every section represents a separate object in the image.
4. **Object Detection:** Object recognition is the task of recognising things in a picture and is frequently utilized in security and surveillance applications. For object detection, many alternative methods may be utilized, but the most prevalent way is to use Deep Learning designs, notably Convolutional Neural Networks. (CNNs).
5. **Image Compression:** Compressing images is the technique of lowering the file size for an image while aiming to keep the image's quality. This is done to conserve storage space, particularly when running picture Process algorithms in mobile or connected devices, or to minimise the bandwidth needed to send the picture.
6. **Image manipulation:** image manipulation refers the process of changing the look of an image. This may be needed for a variety of reasons, like deleting an undesired object from a picture or inserting a thing that was not previously present. Graphic designers frequently employ this technique for creating posters, films, and various other media.



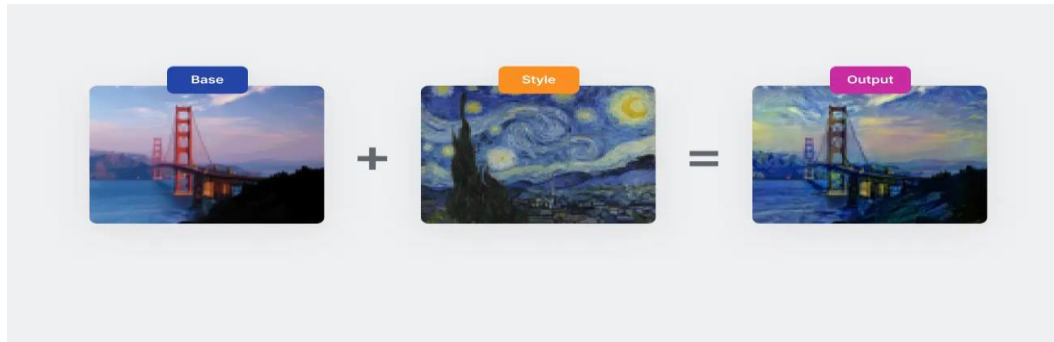


Figure 3.8 Example of Image manipulation

7. **Image generation:** Another essential task in the processing of images is picture synthesis, particularly for Deep Learning systems that require vast amounts of labelled information to train. Image generating methods often employ Generative Adversarial Networks (GANs), an alternative to neural network design.
8. **Image-to-Image translation:** The purpose of image-to-image translation is to learn the relationship between an input picture and the resultant picture using a training set of matched image pairings. A free-hand drawing, for example, can be used as an input in order to generate an accurate representation of the item portrayed in the drawing for the output, as illustrated below.



Figure 3.9 Example of Image-to-Image translation

### 3.7 Applications

Digital image processing has a live influence on almost every industry and is developing with time and new technology.

**1) Image sharpening and restoration:** It means the process of changing the feel and look of a picture. It effectively manipulates photos to produce the desired result. It consists of picture conversion, sharpening, blurring, edge detection, retrieval, and identification.

**2) Medical Field:** There are many medical uses that rely on the operation of the processing of digital images.

- Imaging using gamma rays
- PET scan
- X-Ray Technology
- CT scan for medical purposes
- ultraviolet imaging

**3) Robot vision:** Several robotic robots are used in digital image processing. Robots locate their paths using methods for image processing, such as the hurdle detecting robot or line follower robot.

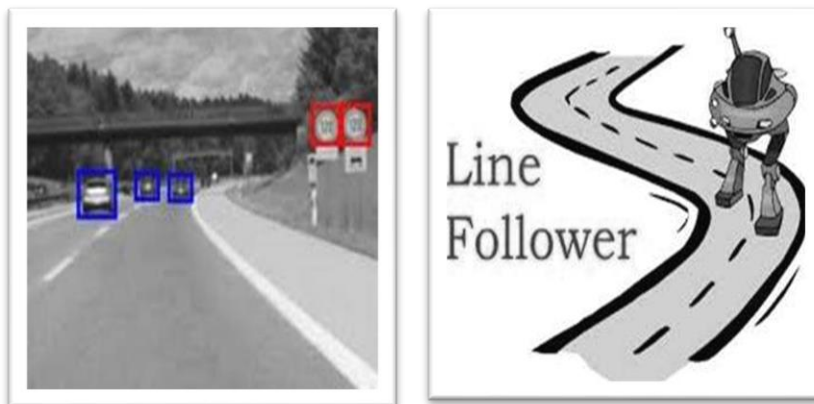


Figure 3.10 Hurdle detection robot and Line follower robot.

**4. Military and Security purposes:** Digital image processing is now widely used in military and security applications such as tiny detection and observing, missile direction, vehicle navigating, wide-area monitoring, and automatic/aided target recognition

## CHAPTER IV

### SPATIAL DOMAIN DENOISING APPROACH

#### 4.1 Spatial Domain Processing

A 2D matrix can be utilized for modelling a picture, with each member representing pixel intensity. Spatial Domain refers to the state of two-dimensional matrices that reflect the intensity spectrum of a picture. It can be shown as illustrated. in fig. 4.1.

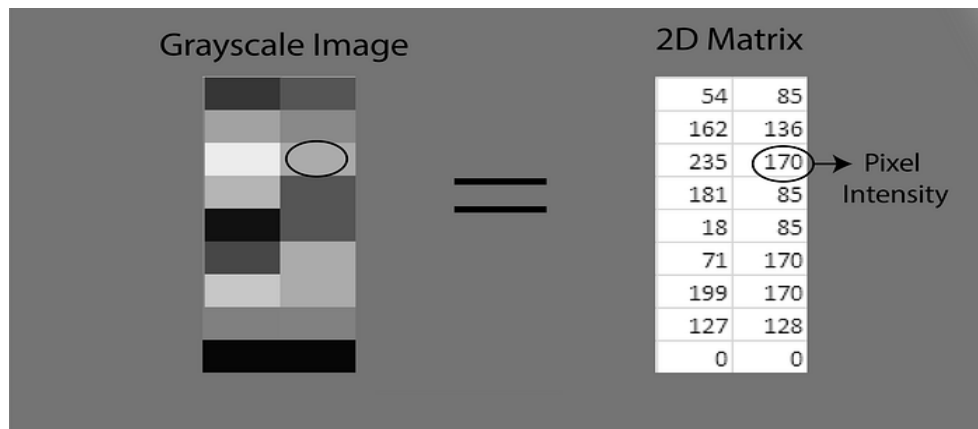


Figure 4.1 Illustration of Spatial Domain

The spatial domain of the RGB image can be expressed by a 3D vectors of 2D matrices. As illustrated in fig. 4.2, each 2D matrix holds intensity values for a single colour. Every pixels intensity can be expressed as  $I(x,y)$ , and  $x,y$  is the pixel's co-ordinate in a 2D matrix. This value performs a variety of operations. For instance, the operation T (say, adding 5 to all pixels) is performed in  $I(x,y)$ , which indicates that the value of each pixel is increased by 5. This can be expressed as,

$$I'(x,y) = T[I(x,y)]$$

where,  $I'(x,y)$  is the new intensity after adding 5 to  $I(x,y)$ .

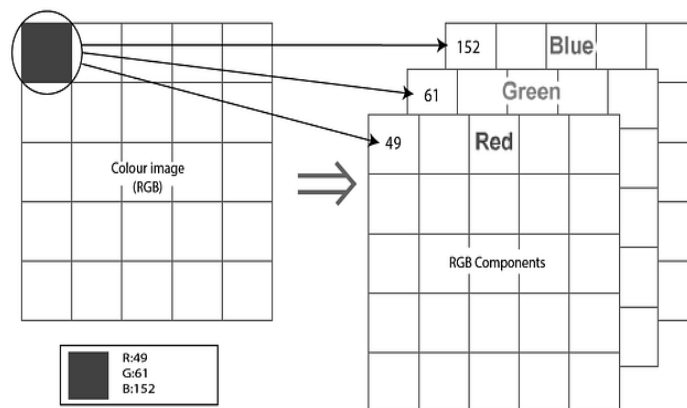


Figure 4.2 Spatial domain for color image (RGB)

## 4.2 Spatial Filters

The spatial filtering technique is applied directly to the image's pixel level. Masks are typically thought of as being larger so that they have a specific centre pixel. The mask is positioned on the image so that its centre traverses every pixel. Spatial filtering is an image processing technique that modifies a pixel's intensity in accordance with the brightness of its neighbouring pixels.

The filtering method involves moving the filter into the image functions  $f(x, y)$  point by point until the center in the filtering coincides with the point.  $(x, y)$ . At every point  $(x, y)$ , the filter's response is determined according to the particular material of the filters via a predefined relationship termed 'template'.

If each pixel in the neighborhood is determined as a linear process, it is known to as 'linear spatial domain filtering'; otherwise, it is referred to as 'nonlinear spatial domain filtering'. Figure 4.3 depicts the spatial filtering method utilizing a 3 3 template. (also known as a filter, kernel, or window).

In linear spatial filtering, the filter coefficients form the weighted pattern. For example, the response 'R' to the template for Figure 4.3 is:

$$R = w(-1, -1) * f(x - 1, y - 1) + w(-1, 0) * f(x - 1, y) + \dots + w(0, 0) * f(x, y) + \dots + w(1, 0) * f(x + 1, y) + w(1, 1) * f(x + 1, y + 1)$$

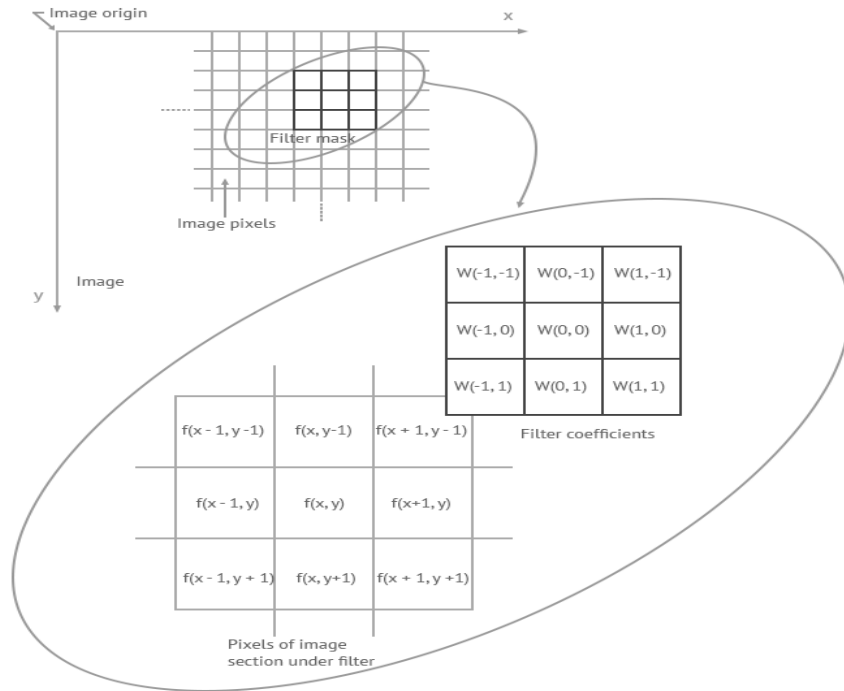


Figure 4.3 Filtering in spatial domain

In mathematics, this is known as element-wise matrix multiplication. The output response of the filter with a dimension of  $(2a+1, 2b+1)$  may be determined with a function as follows:

$$g(x, y) = \sum_{s=-a}^a \sum_{t=-b}^b w(s, t) f(x + s, y + t)$$

Spatial filtering is categorized generally as follows:

1. Smoothing spatial filter: It is used for picture blurring and noise reduction.
2. Sharpening spatial filter: It is used for edge highlighting and to remove blurring from pictures.

The below section explains some of the most used filters.

### 4.3 Mean Filter

A linear spatial filter is composed of the mean of each pixel in the selection mask's general neighborhood. The idea is that it will average remove the grey levels for the surrounding region of a picture as determined by the filter's mask, substituting the value of each pixel. This is a regional averaging process and one of the most basic linear filters. The average for every one of the values for the local vicinity is used to replace the value for every pixel. If  $f(i,j)$  represents a noisy image, then the smoother image  $g(x,y)$  may be calculated as follows:

$$g(x,y) = 1/n \sum_{(i,j) \in S} f(i,j)$$

Where S is a neighbourhood of (x,y) and n is the number of pixels in S.

E.g.: - 3x3 mean filtering,

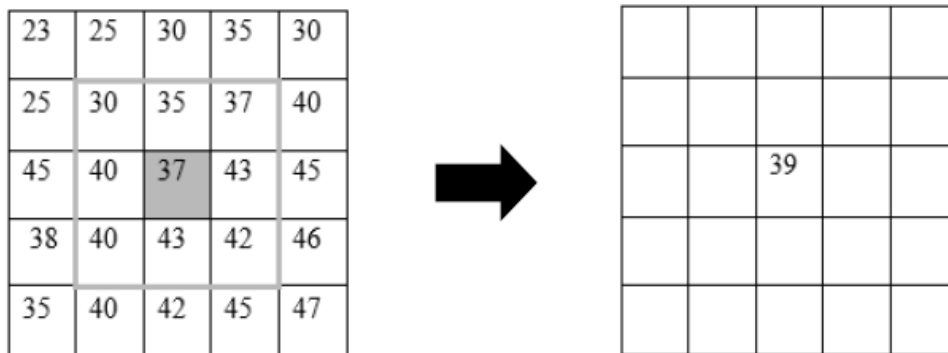


Figure 4.4 3x3 Mean Filtering

#### 4.3.1 Types of Mean filter

1. **Averaging filter:** It is used to reduce the amount of visual detail. Each coefficient is the same.
2. **Weighted averaging filter:** This involves multiplying the pixels by various coefficients. A larger value than the standard filter is multiplied by the centre pixel.

#### **4.4 Adaptive Weighted Mean Filter:**

Adapted weighted mean filtration is used to find noise spots within the grey gold picture in order to eliminate the noise points discovered through the modified means filter technique. This approach may be used to locate noise spots, delete them, and then perform the weighted procedure.

Adaptive weighted mean filtering consists of two steps:

1. do noise detection for the picture
2. The detected noise spots are filtered.

#### **4.5 Median Filter**

The median filter, like the average filter, examines each pixel in the picture in turn and compares it to its neighbours to determine if it is typical of its surroundings. Rather than merely replacing the value of a pixel with the average of its neighbors, it replaces it by the median of those values.

The median is derived by first statistically ranking all of the pixel values in the surrounding neighbourhood and then replacing the pixel under examination with the middle pixel value. (If the neighbourhood under consideration contains an even number of pixels, the average of the two middle pixel values is used.) An example computation can be seen in Figure 4.5.

Figure 4.5: Finding the median value for a pixel neighbourhood. As shown, the central pixel's value of 150 is not typical for the surrounding pixels and is substituted by the median value of 124. A 3x3 square neighbourhood is utilised in this example; bigger neighbourhoods will result in more severe smoothing.



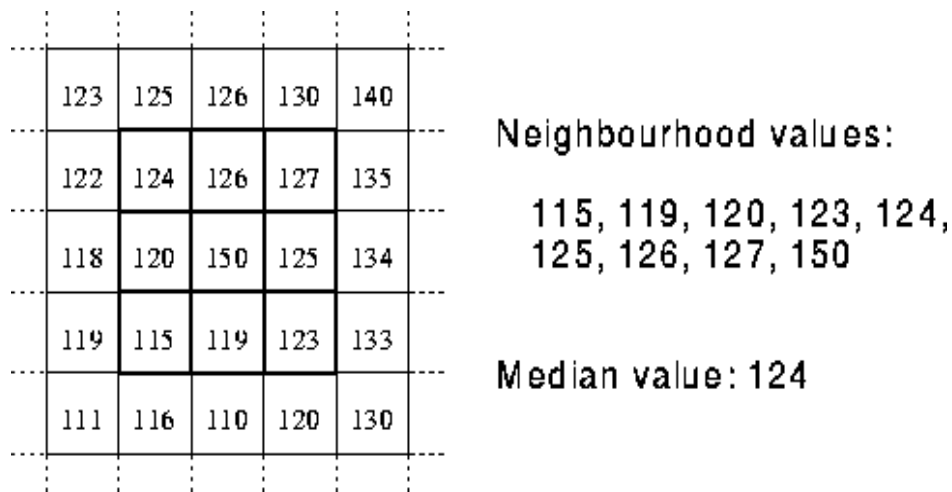


Figure 4.5 Median filtering

### 4.6 Adaptive Weighted Median Filter

An adapted median filter conducts spatial processing on a picture to decrease noise. The mask compares every single pixel in the picture to the pixels around it. When one of the values of a pixel is considerably different from most of the neighboring pixels, that pixel is considered noise. The noisy pixel is then replaced by the average values from the surrounding pixels using the filtering method. This technique is repeated until all of the noise pixels on the picture have been eliminated.

### 4.7 Non-Local Mean Filter

That non-local means filtering reduces noise in the input image while maintaining the clarity of strong edges such as the man's silhouette and buildings. This function effectively smooths textured portions of the image, like grass in the foreground, leading to less detail than the chaotic image.

Non-local means an image processing method used for picture denoising. Non-local means filtering, as opposed to "local mean" filters, that use the mean value of a set of

pixels around a target pixel for smoothing the picture, takes the mean value of every pixels of the image, weighted on how similar those pixels are with the target pixel. When compared to local mean methods, this results in substantially improved post-filtering clarity and less loss of picture detail.

# CHAPTER V

## METHODOLOGY

### 5.1 Introduction

Here, our goal is to remove noise and, through a sequence of actions, produce an image that is close to the original image. In this methodology, we outline the steps that were done in order to accomplish the objective. We begin with the adaptive two-stage threshold technique, which enhances COVID-19 detection accuracy by lowering the error in estimating noisy signal points. Then, based on a specific optimisation methodology, we employ the weighted median filter picture denoising method. This is done to find suitable pixel value that would replace the noise point in order to reconstruct the original image. One of the key components in this whole process is the optimization techniques which help in getting a better MSE, PSNR and IEF values. The ones we considered here are Aquila Optimizer and Arithmetic Optimization Algorithm. This is the whole implementation process considered.

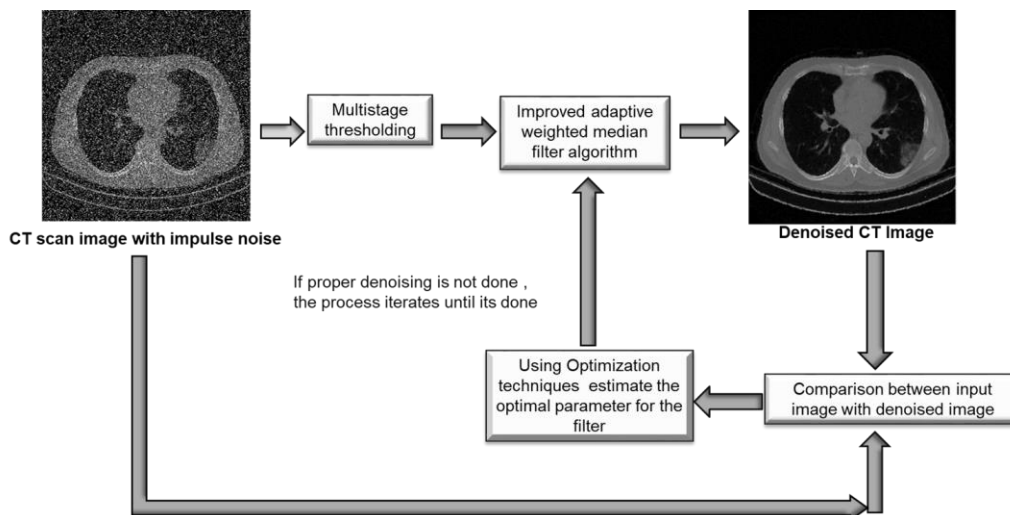


Figure 5.1 Flowchart of the process in brief

## 5.2 Adaptive Multi-level Thresholding

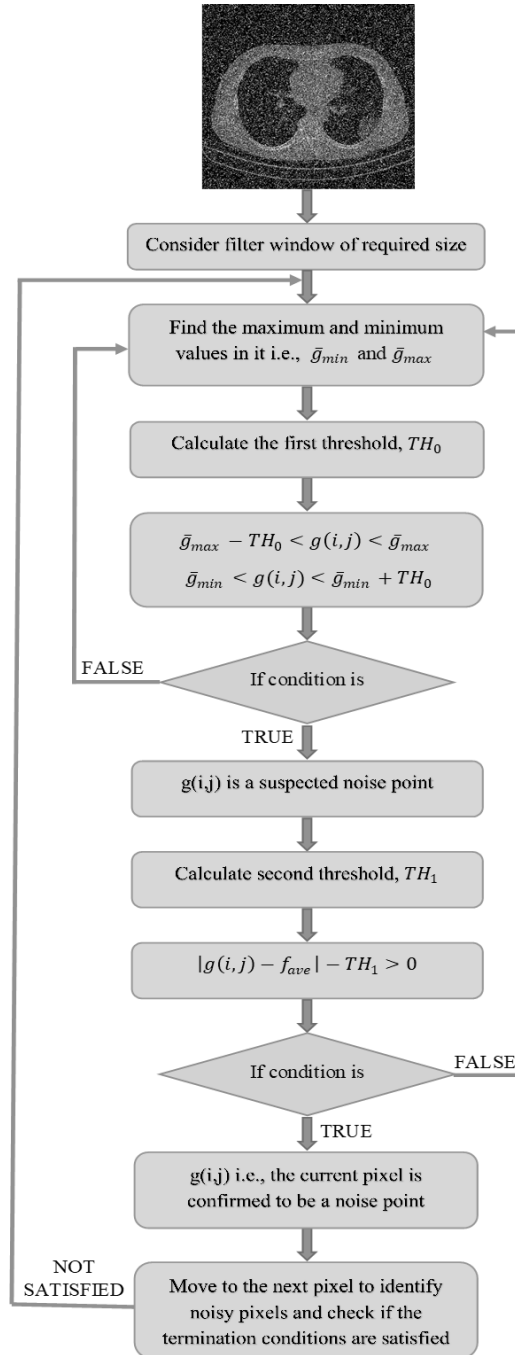


Figure 5.2 Flowchart of Adaptive multi-level thresholding

Noise can readily confound the early COVID-19 CT picture. The COVID-19 lesion signals can readily be misdiagnosed using the conventional extreme noise points judgement. For the single threshold filtering approach, the pixel whose value exceeds the current threshold will be regarded as noise. The possibility of identifying errors in noise may therefore be increased by using a single threshold method. As a result, we use two-level thresholding to boost noise detection accuracy.

### 5.2.1 Methodology

The initial step in the noise point detection process is the calculation of the threshold, or  $TH_0$ . Its objective is to locate potential noise sources which is done using equation (1) for  $TH_0$ ,

$$\begin{aligned}
TH_0 = & \frac{1}{n} |\sum_{m=-2}^2 \sum_{n=-2}^2 [g(i+m, j+n) - g_{med}]|^{\frac{1}{2}+} \\
& \frac{1}{n} |\sum_{m=-2}^2 \sum_{n=-2}^2 [g(i+m, j+n) - g_{ave}]|^{\frac{1}{2}+} \\
& \frac{1}{n} |\sum_{m=-2}^2 \sum_{n=-2}^2 [g(i+m, j+n) - \bar{M}_U]|^{\frac{1}{2}+} \\
& \frac{1}{n} |\sum_{m=-2}^2 \sum_{n=-2}^2 [g(i+m, j+n) - \bar{M}_D]|^{\frac{1}{2}+} \\
& \frac{1}{n} |\sum_{m=-2}^2 \sum_{n=-2}^2 [g(i+m, j+n) - \bar{M}_L]|^{\frac{1}{2}+} \\
& \frac{1}{n} |\sum_{m=-2}^2 \sum_{n=-2}^2 [g(i+m, j+n) - \bar{M}_R]|^{\frac{1}{2}+}
\end{aligned} \tag{1}$$

The variables n and m stand for the filter window's length and width, respectively (the length and width are equal), while  $g(i, j)$  stands for the current pixel's grey value. The grey values of all the pixels in the filter window are represented by the terms  $g_{med}$  and  $g_{ave}$ , respectively. On the point's left, right, top, and bottom sides (i,j), four neighbourhood rectangle windows of  $5 \times 2$  and  $2 \times 5$  are formed, and the four neighbour windows' respective grey average values are defined as  $\bar{M}_U$ ,  $\bar{M}_D$ ,  $\bar{M}_L$  and  $\bar{M}_R$ , as shown below.

$$\bar{M}_U = \frac{\sum_{k=-2}^{-1} \sum_{l=-2}^2 g(i+k, j+l)}{5 \times 2} \tag{2}$$

$$\bar{M}_D = \frac{\sum_{k=-2}^2 \sum_{l=-2}^{-1} g(i+k, j+l)}{5 \times 2} \tag{3}$$

$$\bar{M}_L = \frac{\sum_{k=1}^2 \sum_{l=-2}^2 g(i+k, j+l)}{5 \times 2} \quad (4)$$

$$\bar{M}_R = \frac{\sum_{k=-2}^2 \sum_{l=1}^2 g(i+k, j+l)}{5 \times 2} \quad (5)$$

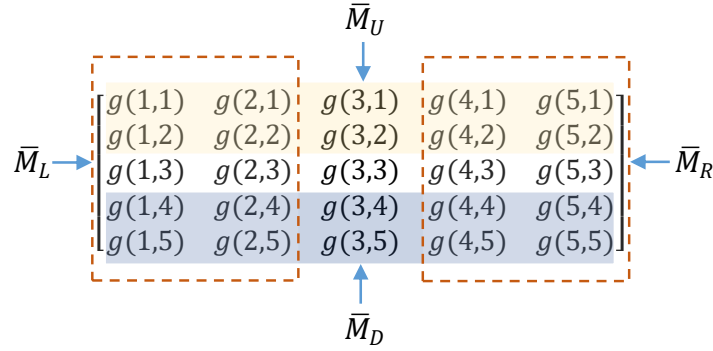


Figure 5.3 representation of filter window of size  $5 \times 5$

Figure 5.1 represents the filter window and the way in which four neighbourhood windows considered for the calculation. Then the adaptive minimum,  $\bar{g}_{min}$  and adaptive maximum,  $\bar{g}_{max}$  are calculated. It is then that the below equations are checked for the suspected noise points.

$$\bar{g}_{max} - TH_0 < g(i,j) < \bar{g}_{max} \quad (6)$$

$$\bar{g}_{min} < g(i,j) < \bar{g}_{min} + TH_0 \quad (7)$$

If any of the following conditions is satisfied then that particular point,  $g(i,j)$  is suspected to be a noise point. Next, we proceed to the following phase and determine the second threshold value  $TH_1$ .

Calculation of threshold,  $TH_1$ : The second stage of noise point detection is this threshold. When a point is thought to be noise, the filter window's average grey value for all pixels is determined. The current point must be replaced with the value obtained

using the adaptive weighted median filter and optimizer, which is done in the following steps, if the grey value of the point differs noticeably from the average value. The calculation of the second threshold,  $TH_1$ , is made possible by the second threshold's more precise assessment of the suspected noise location.:

$$TH_1 = \varphi p = (F_1 + F_2) \times \frac{N_{pn}}{n \times n} \quad (8)$$

The regulating factor of threshold is the variable  $\varphi$ ,  $TH_1$ ,  $\varphi = F_1 + F_2$ , the expression of  $F_1$  and  $F_2$  is:

$$F_1 = \frac{1}{n \times n} \left| \sum_{k=-2}^2 \sum_{l=-2}^2 [g(i+k, j+l) - g_{med}] \right| \quad (9)$$

$$F_2 = \frac{1}{n \times n} \left| \sum_{k=-2}^2 \sum_{l=-2}^2 [g(i+k, j+l) - F_1] \right| \quad (10)$$

the expression is, here  $p$  is the noise density of the image,  $p = \frac{N_{pn}}{n \times n}$ ;  $N_{pn}$  reflects how many noise points there are in the window. Then the below condition is checked for.

$$|g(i, j) - g_{ave}| - TH_1 > 0 \quad (11)$$

If the above condition is satisfied then the suspected noise point is in actual a noise point, else it is not a noise point. In order to achieve adaptive threshold selection in the same image under varying noise densities, the threshold value is related to the noise density and the threshold  $TH_1$  grows as the noise density increases. In this manner, the noise sites in the noise-affected CT picture are detected, enabling effective noise removal. Now the next task is to replace these identified noise points with appropriate values to get the actual image.

### 5.3 Meta heuristic Optimization Algorithm

The methods used to get the optimal answer for a system's provided parameters are known as optimisation algorithms. Using traditional mathematical approach makes it

hard to find the best solution in current scenario where problems vary in terms of both complexity and type. This being the reason optimization algorithms are widely being used for the same. Out of many existing algorithms meta heuristic optimization algorithms are widely used, as unlike heuristic algorithms they are not problem-specific. These algorithms use two search phases to find the optimal solution.

1. Exploration Phase.
2. Exploitation Phase.

The first phase refers to finding parameter in a diverge search space and the second phase refers to finding parameter in converge search space. This lastly gives out the possible best solution. Two of such algorithms employing these search techniques used in this project are ‘Aquila Optimizer’ and ‘Arithmetic Optimization Algorithm’. Here we’re using these techniques to find parameter values. So, hereby solutions of AO and AOA will be referred to as parameters.

## **5.4 Aquila Optimizer**

In this paper we’ve considered two population based meta-heuristic algorithms with one of them being Aquila optimizer. Once the noise points are detected they are now supposed to be replaced with the proper gray values so as to remove noise and yield a proper CT image helpful for diagnosis. The above said is implemented with the help of a filter we’ve considered, which is explained in the further sections. These optimization techniques are actually used in combination with the filter so as to find better parameter values. These values are then given to filter for better noise point replacement. This is done so as to improvise the result given by filter alone. This technique is inspired from a bird ‘Aquila’, considering its varied hunting techniques depending on certain circumstances. The four methods of hunting are:

1. High soar with a vertical stoop.
2. Contour flight with short glide attack.
3. Low flight with a slow descent attack.
4. Walk and grab prey method.



### 5.4.1 Methodology:

Meta-heuristic algorithms employ two stages for searching mechanisms i.e., exploration and exploitation. Each stage in this technique is explained as 2 steps based on Aquila's hunting techniques. These 4 stages differ in the region covered by each of them. AO shifts between the exploration and exploitation phase using the condition. If it is accurate, AO is in the exploration phase; if not, it is in the exploitation phase.

$$t \leq \left(\frac{2}{3}\right) * T$$

The current iteration (t) and maximum iteration (T) are shown, correspondingly. Initially, a set of optimization parameters (P) is generated using the specified upper and lower bound values. Here we considered LB=1, UB=10, Dim=2.

$$P = \begin{bmatrix} p_{1,1} & \cdots & p_{1,j} & p_{1,1} & p_{1,Dim} \\ p_{2,1} & \cdots & p_{2,j} & \cdots & p_{2,Dim} \\ \cdots & \cdots & p_{i,j} & \cdots & \cdots \\ \vdots & \vdots & \vdots & \vdots & \vdots \\ p_{N-1,1} & \cdots & p_{N-1,j} & \cdots & p_{N-1,Dim} \\ p_{N,1} & \cdots & p_{N,j} & p_{1,1} & p_{N,Dim} \end{bmatrix} \quad (12)$$

In each iteration, the obtained best parameter so far is determined to be the optimal parameter value. This set of parameter values is obtained using equation (13) given below.

$$P_{i,j} = rand \times (UB_j - LB_j) + LB_j, \quad i = 1, 2, \dots, N \quad j = 1, 2, \dots, Dim \quad (13)$$

These AO parameter values then keep on updating as the algorithm proceeds searching from a diverge search space to a converge search space to obtain optimal parameters,  $\eta_1$  and  $\eta_2$ .

## 1. Expanded Exploration ( $P_1$ ):

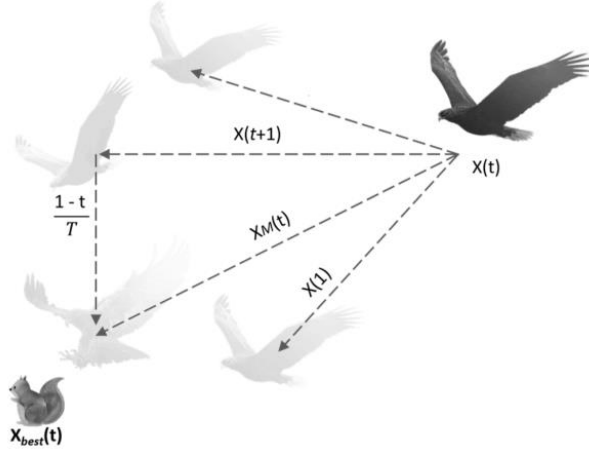


Figure 5.4 The behaviour of the Aquila high soar with the vertical stoop.

This is the first skill that borrows from Aquila's high soar with vertical stoop manoeuvre. This allows it to identify the prey area and choose the ideal hunting location. Similar to how it was done in this case, the AO extensively explored the search space from a high altitude. It is shown mathematically as,

$$P_1(t+1) = P_{best}(t) \times \left(1 - \frac{t}{T}\right) + (P_M(t) - P_{best}(t) * rand) \quad (14)$$

here,  $P_1(t+1)$  is the parameter value of next iteration of  $t$ .  $P_{best}(t)$  is the best parameter found up to this iteration.,  $t$ .  $\left(1 - \frac{t}{T}\right)$  controls the expanded search. Current and maximum iterations are  $t$  and  $T$ , respectively. A random number between 0 and 1 is called  $rand$ .  $P_M(t)$  is the current parameters' mean value connected at  $t^{th}$  iteration which is given as,

$$P_M(t) = \frac{1}{N} \sum_{i=1}^N P_i(t), \quad \forall j = 1, 2, \dots, Dim \quad (15)$$

where,  $N$  is the population size, and  $Dim$  is the problem's dimension size.

## 2. Narrowed exploration ( $P_2$ ):

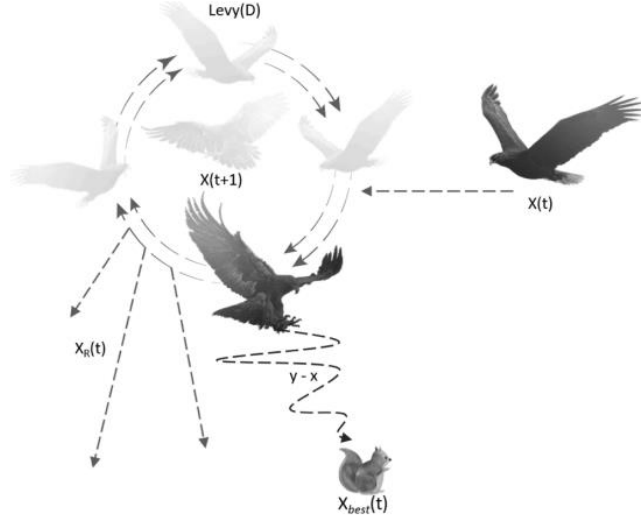


**Figure 5.5** The behaviour of the Aquila contour flight with short glide attack.

The second approach is modelled after the contour flying with brief glide attack of the aquila. Similar to how Aquila prepares the terrain before attacking by circling above its victim. In order to prepare for the attack, AO carefully examines the chosen area of the intended prey. It is denoted mathematically as,

$$P_2(t + 1) = P_{best}(t) \times Levy(D) + P_R(t) + (y - x) * rand \quad (16)$$

where,  $P_2(t + 1)$  is the variable that the upcoming iteration of  $t$ 's parameter, as produced by the second search procedure, will have ( $P_2$ ).  $P_R(t)$  is a random parameter chosen between  $[1 N]$ .  $D$  is the dimension space, and  $Levy(D)$  is the levy flight distribution function, which is calculated as given below.

$$Levy(D) = s \times \frac{u \times \sigma}{|v|^{\frac{1}{\beta}}} \quad (17)$$

where  $s$  is a constant with a fixed value of 0.01 and  $u$  and  $v$  are random values between 0 and 1.  $\sigma$  is calculated using,

$$\sigma = \left( \frac{r(1 + \beta) \times \sin\left(\frac{\pi\beta}{2}\right)}{\Gamma\left(\frac{1 + \beta}{2}\right) \times \beta \times 2^{\left(\frac{\beta-1}{2}\right)}} \right) \quad (18)$$

where  $y$  and  $x$  are variables that are used to portray the spiral shape in the search, and which are calculated as follows. where is a constant value that is equal to 1.5.

$$x = r \times \sin \theta \quad (19)$$

$$y = r \times \cos \theta \quad (20)$$

Where,

$$r = r_1 + U \times D_1 \quad (21)$$

$$\theta = -\omega \times D_1 + \theta_1 \quad (22)$$

$$\theta_1 = \frac{3 \times \pi}{2} \quad (23)$$

For a set number of search cycles,  $r_1$  takes a value between 1 and 20, and  $U$  is a tiny value fixed at 0.00565.  $D_1$  consists of integers from 1 to the search space's length (Dim), and is a tiny value set to 0.005.

### 3. Expanded exploitation ( $P_3$ ):

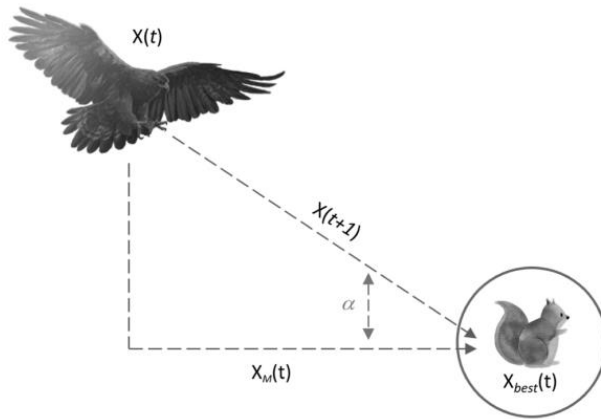


Figure 5.6 The behaviour of the Aquila low flight with slow descent attack.

In the third approach (X3), the aquila descends vertically with an initial attack to ascertain the prey reaction after the prey region has been precisely designated and the aquila is prepared for landing and attacking. Low flying with gradual descent assault is the name of this technique. Here, AO takes advantage of the target's chosen location to approach its victim and attack. It is mathematically represented as,

$$P_3(t + 1) = (P_{best}(t) - P_M(t)) \times \alpha - rand + ((UB - LB) \times rand + LB) \times \delta \quad (24)$$

Where,  $P_3(t + 1)$  is the parameter value of next iteration of t, generated using  $P_3$ .  $P_{best}(t)$  is the best parameter value obtained till  $t^{th}$  iteration.  $P_M(t)$  is the current parameter's mean value i.e., at  $t^{th}$  iteration. The upper and lower bounds for the problem under consideration are UB and LB, respectively. A random number between 0 and 1 is called rand.  $\alpha$  and  $\delta$  are valued to 0.1 and these are exploitation adjustment parameters.

#### 4. Narrowed exploration ( $P_4$ ):

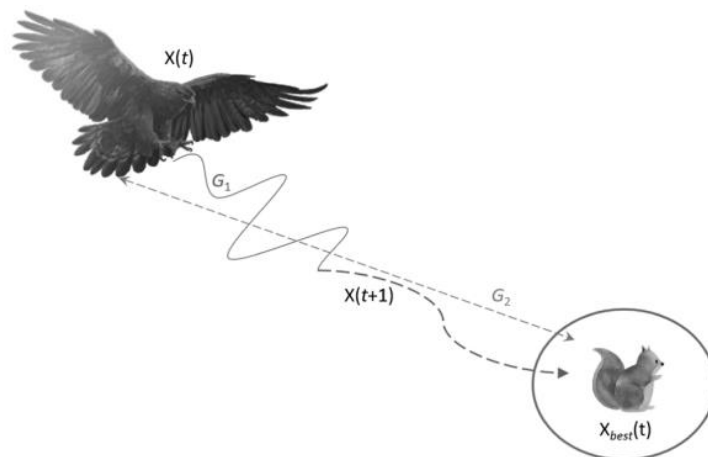


Figure 5.7 The behaviour of the Aquila walk and grab prey.

The Aquila approaches its prey and assaults it throughout the landscape in accordance with its stochastic motions, which is the model for the fourth method. The AO then engages the prey in the final place. It is denoted mathematically as,

$$P_4(t + 1) = QF \times P_{best}(t) - (G_1 \times P(t) \times rand) - G_2 \times Levy(D) + rand \times G_1 \quad (25)$$

Where,  $P_4(t + 1)$  is the next parameter of current iteration, t. The quality factor, or QF, is employed to balance the search strategies. G2 illustrates the decreasing values from 2 to 0 that make up the flight slope of the AO used to track the prey during its escape from the starting site (1) to the final position (t). G1 refers to a variety of AO motions used to track the prey while it runs away. A random number between 0 and 1 is called rand.  $Levy(D)$  is the Levy distribution function.

$$QF(t) = t^{\frac{2 \times rand - 1}{(1-T)^2}} \quad (26)$$

$$G_1 = 2 \times rand - 1 \quad (27)$$

$$G_2 = 2 \times \left(1 - \frac{t}{T}\right) \quad (28)$$

Thus, at the end of this AO algorithm we get the best value of Optimization parameters with MSE as objective function. Below is a flowchart defining the flow of AO algorithm.

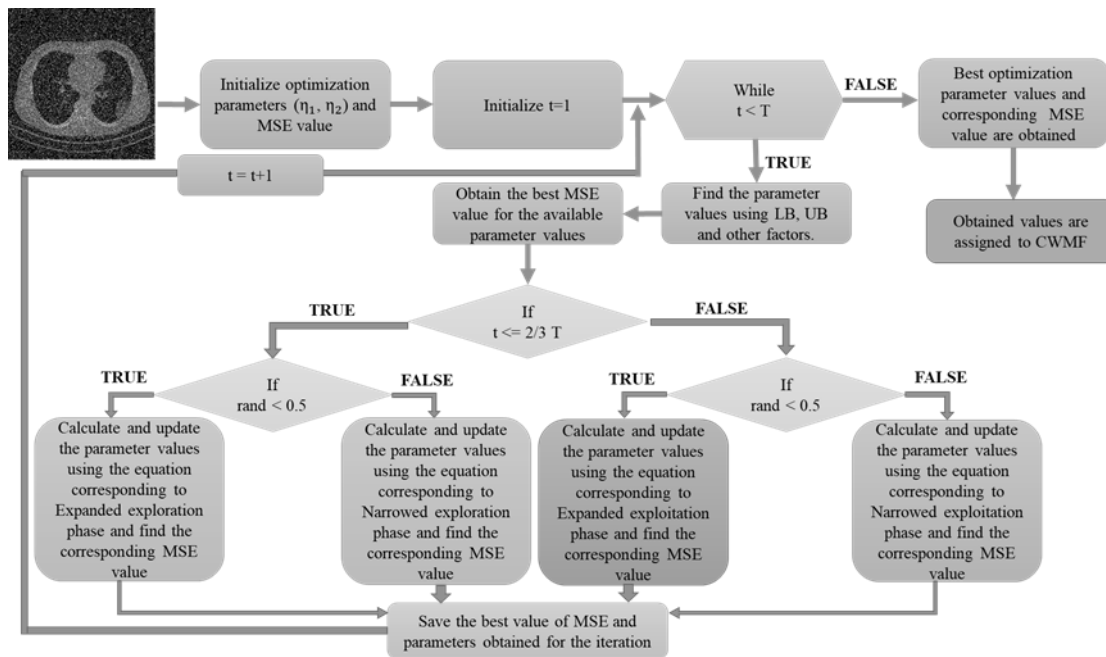


Figure 5.8 Flow chart of AO technique

## 5.5 Arithmetic Optimization Algorithm

The exploration and exploitation phase is carried out via the Arithmetic Optimization Algorithm (AOA), which makes use of the distribution behaviour of the four main arithmetic operators in mathematics: Multiplication (M), Division (D), Subtraction (S), and Addition (A). As was already established, the conventional computation methods typically employed to examine numbers are arithmetic operators. Here, a set of candidate alternatives is analysed mathematically to identify the best element based on a set of predetermined criteria. (parameters). This meta-heuristic technique uses population data to solve optimisation issues without figuring out their derivatives.

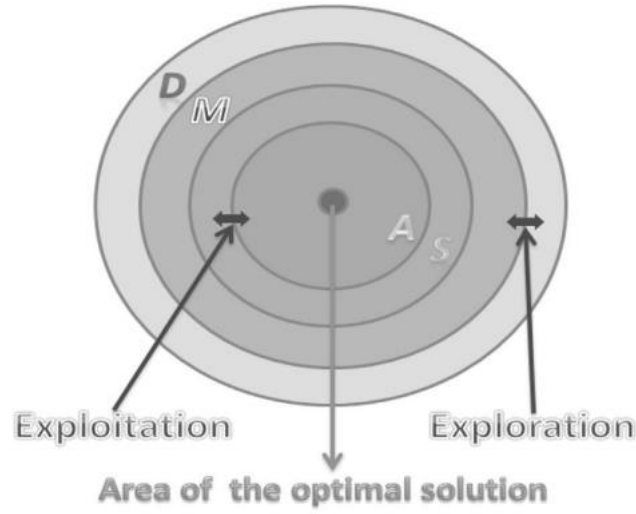


Figure 5.9 Arithmetic operator hierarchy (dominance decreases from top-down).

### 5.5.1. Methodology

Initially, a set of optimization parameters ( $S$ ) is generated utilising the upper and lower bound values provided for the considered problem. Here we considered  $LB=1$ ,  $UB=10$ .

$$S = \begin{bmatrix} S_{1,1} & \cdots & \cdots & S_{1,j} & S_{1,n-1} & S_{1,n} \\ S_{2,1} & \cdots & \cdots & S_{2,j} & \cdots & S_{2,n} \\ \cdots & \cdots & \cdots & \cdots & \cdots & \cdots \\ \vdots & \vdots & \vdots & \vdots & \vdots & \vdots \\ S_{N-1,1} & \cdots & \cdots & S_{N-1,j} & \cdots & S_{N-1,n} \\ S_{N,1} & \cdots & \cdots & S_{N,j} & S_{N,n-1} & S_{N,n} \end{bmatrix} \quad (29)$$

In each iteration, the obtained best parameter value so far is determined to be the best optimal parameter value. In order to choose the search space, the Math Optimizer Accelerated (MOA) function is a coefficient. (i.e., exploration or exploitation). It is determined as,

$$MOA(C\_Iter) = Min + C\_Iter \times \left( \frac{Max - Min}{M\_Iter} \right) \quad (30)$$



Where,  $MOA(C\_Iter)$  represents the function value at the current iteration, as determined by the previous equation.  $C\_Iter$  between 1 and the maximum number of iterations, represents the current iteration  $M\_Iter$ . The accelerated function's minimum and maximum values are indicated by the letters Min and Max, respectively.

Then, as the algorithm moves from a diverge search space to a converge search space to find the best parameter values, these parameter values continue to change. The steps involved in a search in AOA are as follows:

### 1. Phase-1 (Exploration):

The mathematical computations employing either the Division (D) operator or even the Multiplication (M) operator obtained highly scattered values or decisions that commit to the exploration search process, according to the Arithmetic operators. Contrary to other operators (S and A), these operators (D and M) are difficult to approach the target due to their high dispersion, as seen in Figure 5.9. Following multiple attempts, the exploration search finds the almost ideal parameter. (iterations). Additionally, at this level of optimization, the exploration operators (D and M) were operated to support the exploitation stage of the search process by improving communication between them.

This phase is executed when  $r_1 > MOA$ . Figure 5.9 demonstrates how the employed operators move closer to the ideal region. The two primary search techniques—Division (D) search strategy and Multiplication search strategy—are modelled in the equation below. The exploration operators of AOA explore the search area randomly on different regions and seek to find a better parameter based on these two search strategies. The Math Optimizer accelerated (MOA) function conditions this stage of the search on the fact that  $r_1 > MOA$  ( $r_1$  is a random number). In this phase, much like in the first line of the equation below, the first operator (D) is conditioned by  $r_2 < 0.5$ , and the second operator (M) will be disregarded until the first operator completes its present duty. If not, the second operator (M) will be employed in place of the D to complete the present task ( $r_2$  is a random number).

$$S_{i,j}(C_{Iter} + 1) = \begin{cases} best(s_j) \div (MOP + \epsilon) \times ((UB_j - LB_j) \times \mu + LB_j), & r_2 < 0.5 \\ best(s_j) \times MOP \times ((UB_j - LB_j) \times \mu + LB_j), & otherwise \end{cases} \quad (31)$$

where  $s_i(C_{Iter} + 1)$  indicates the  $i^{th}$  parameter in the next iteration,  $s_{i,j}(C_{Iter})$  denotes the  $j^{th}$  position of the  $i^{th}$  parameter at the current iteration, and  $best(s_j)$  is the  $j^{th}$  position in the best-obtained parameter so far.  $\epsilon$  is an extremely tiny integer.,  $UB_j$  and  $LB_j$  signify the  $j^{th}$  position's upper bound value and lower bound value, respectively.  $\mu$  is a control parameter that can be used to modify the search process. Its value is fixed at 0.5 for the paper under consideration.

$$MOP(C_{Iter}) = 1 - \frac{C_{Iter}^{1/\alpha}}{M_{Iter}^{1/\alpha}} \quad (32)$$

Where, Math Optimizer probability ( $MOP$ ) is a coefficient,  $MOP(C_{Iter})$  denotes the function value at the *current* iteration, and  $C_{Iter}$  denotes the current iteration and ( $M_{Iter}$ ) denotes the maximum number of iterations.  $\alpha$  is the sensitive parameter, which according to the paper under consideration is fixed at 5, defines the exploitation accuracy over the iterations.

## 2. Phase-2 (Exploitation):

The mathematical calculations utilising either addition (A) or subtraction (S) produced highly dense results, which are related to the exploitation search process, according to the arithmetic operators. The reduced dispersion of these operators (S and A) makes them easier to approach the target than other operators. As a result, the exploitation search finds the almost ideal parameter that can be determined after numerous attempts. (iterations). At this level of optimization, the exploitation operators (S and A) were also used to support the exploitation stage through improved communication.

The MOA function value for the requirement that  $r_1$  is not bigger than the current  $MOA(C_{Iter})$  value is a condition for this phase of searching (exploitation search by executing S or A). When searching for a better parameter in AOA, the exploitation operators (Subtraction (S) and Addition (A)) use two main search

strategies (i.e., Subtraction (S) search strategy and Addition (A) search strategy), which are modelled in the equation below.

$$S_{i,j}(C_{Iter} + 1) = \begin{cases} best(s_j) - MOP \times ((UB_j - LB_j) \times \mu + LB_j), & r_3 < 0.5 \\ best(s_j) + MOP \times ((UB_j - LB_j) \times \mu + LB_j), & otherwise \end{cases} \quad (33)$$

In this phase (first rule in the equation above), the first operator (S) is dependent on  $r_3 < 0.5$  and until this operator completes its present work, the other operator (A) will be ignored. If not, the S will be substituted with the second operator (A) to complete the present task. The partitions from the previous phase's methods are analogous to those in this phase. But exploitation search operators (S and A) frequently make an effort to stay out of the local search region. This process helps exploration search strategies identify the ideal parameter while maintaining the variety of the candidate parameters. In the case of local optima stagnation, especially in the more recent iterations, this portion of the search is quite beneficial.

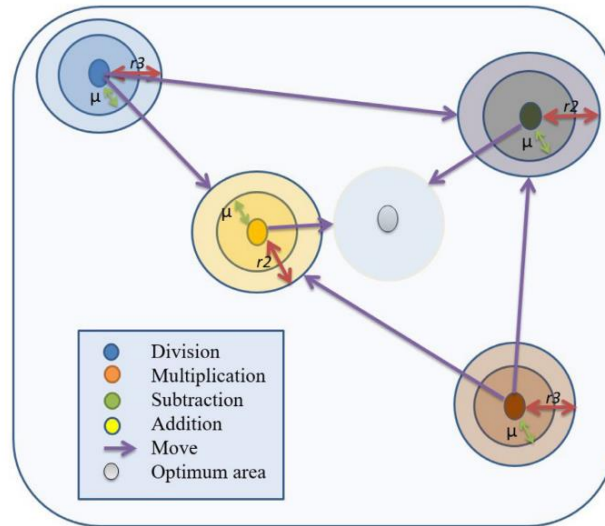


Figure 5.10 Model for moving the math operators in AOA closer to the ideal area.

Figure 5.10 shows how a search parameter in a 2-dimensional search space updates its variables (positions) in accordance with D, M, S, and A. As can be

seen, the final location may fall between a stochastic range defined by the positions of D, M, S, and A inside the search scope. In other notions, the near-optimal parameter's position is estimated by D, M, S, and A, while other parameters update their positions stochastically in its vicinity.

Thus, at the end of this AOA algorithm we get the best value of Optimization parameters with MSE as objective function. Below is a flowchart defining the flow of AOA algorithm.

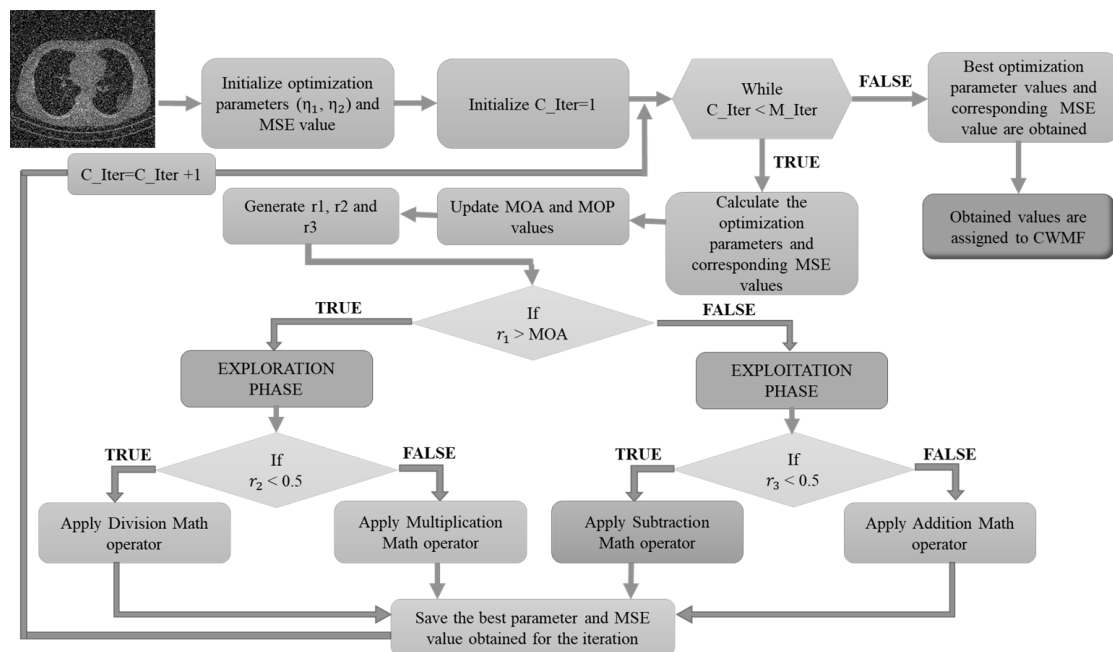


Figure 5.11 Flow chart representing the process flow of AOA algorithm

## 5.6 Center Weighted Median Filter

In more advanced COVID-19 patients, such as those with pneumonia caused by mycoplasma and adenovirus pneumonia, the ground-glass lesions show non-uniformity, and this is similar to the CT imaging of suspected COVID-19 cases. A centre weighted median filter is taken into consideration in order to address the issues that the conventional median filter in denoising poses. As traditional filter performance in noise removal from CT image is unsatisfactory and it also exhibits problem of fuzzy

boundary. This CWM filter accompanied by optimization algorithm gives a proper denoised image in a few iterations.

### 5.6.1 Methodology

Just as the name says we are considering two weighted sub coefficients,  $\gamma_1$  and  $\gamma_2$ . In addition to these we consider two optimization parameters obtained from Optimization algorithm. All together is considered for calculating center weighted median. So now going deep into the process, we first start with the calculation of weights as explained further.

The weighted sub coefficient  $\gamma_1(i, j)$  is set in the weighted coefficient  $\gamma(i, j)$ ,  $\gamma_1(i, j)$  is employed to express the degree to which the current pixel resembles the median pixel.  $g_{med}$  (Illustrating uncontaminated point). The correlation increases as the similarity value decreases. The computation of the weighted sub coefficient  $\gamma_1(i, j)$  is:

$$\gamma_1(i, j) = \frac{\frac{1}{1 + (g(i - r, j - r) - g_{med})^2}}{\sum_{(i-r, j-r) \in W_r} \frac{1}{1 + (g(i - r, j - r) - g_{med})^2}} \quad (34)$$

Here,  $g(i - r, j - r) - g_{med}$  represents the difference of gray values of median pixel and center pixel. While the same part in the denominator with a summation sign to it represents the difference of gray values of median pixel and taken into account are all pixels in the filter window.

Now we are heading to the calculation of next weight,  $\gamma_2(i, j)$  which is as below,

$$\gamma_2(i, j) = \frac{1}{\sum_{(i, j) \in W_r} \sqrt{(s - i)^2 + (t - j)^2}} \quad (35)$$

Here,  $g(s, t)$  represents position coordinates of the pixel traversing through the filter window and  $g(i, j)$  represents position coordinates of the center pixel of the window.  $\gamma_2(i, j)$  gives us the distance of each pixel in the filter window with respect to center pixel. Then we calculate the weighted coefficient  $\gamma(i, j)$

As follows,

$$\gamma(i, j) = \eta_1 \gamma_1(i, j) + \eta_2 \gamma_2(i, j) \quad (36)$$

Where,  $\eta_1$  and  $\eta_2$  are weight parameters, which is optimized by AO or AOA algorithm.  $\gamma_1(i, j)$  and  $\gamma_2(i, j)$  are weighted sub coefficients.  $\gamma(i, j)$  is the improved weight of center weighted filtering. Lastly, we calculate the center weighted median using the formula given below.

$$g(i, j)_{CWM} = \text{median}\{\gamma(i, j) \times g(i, j), g(r, s) \mid g(r, s) \in N_{p(i, j)}^o\} \quad (37)$$

Where,  $\gamma(i, j) \times g(i, j)$  represents the gray value when the weight of  $g(i, j)$  is  $\gamma(i, j)$ ,  $g(i, j)_{CWM}$  is the center weighted median gray value,  $g(i, j)$  represents the gray value of pixel  $p(i, j)$ ,  $N_{p(i, j)}^o$  represents the hollow neighbourhood of pixel  $p(i, j)$ , and  $g(r, s)$  represents the gray value corresponding to all pixels in  $N_{p(i, j)}^o$ . Here, we consider each  $g(i, j)$  pixel gray value repeatedly to certain no. of times and this corresponds to its respective  $\gamma(i, j)$  value. By doing this, we are able to determine the right value to replace the noise-detected pixel with in order to recreate the original image.

Figure 5.12 outlines the whole process. Here as explained earlier we find all the noise points in the image. Then, for first time execution of CWMF a random value for optimization parameters is taken. However, in the next step these values are provided by executing optimization algorithm. This process outlined for a single pixel is repeated for all the pixels.

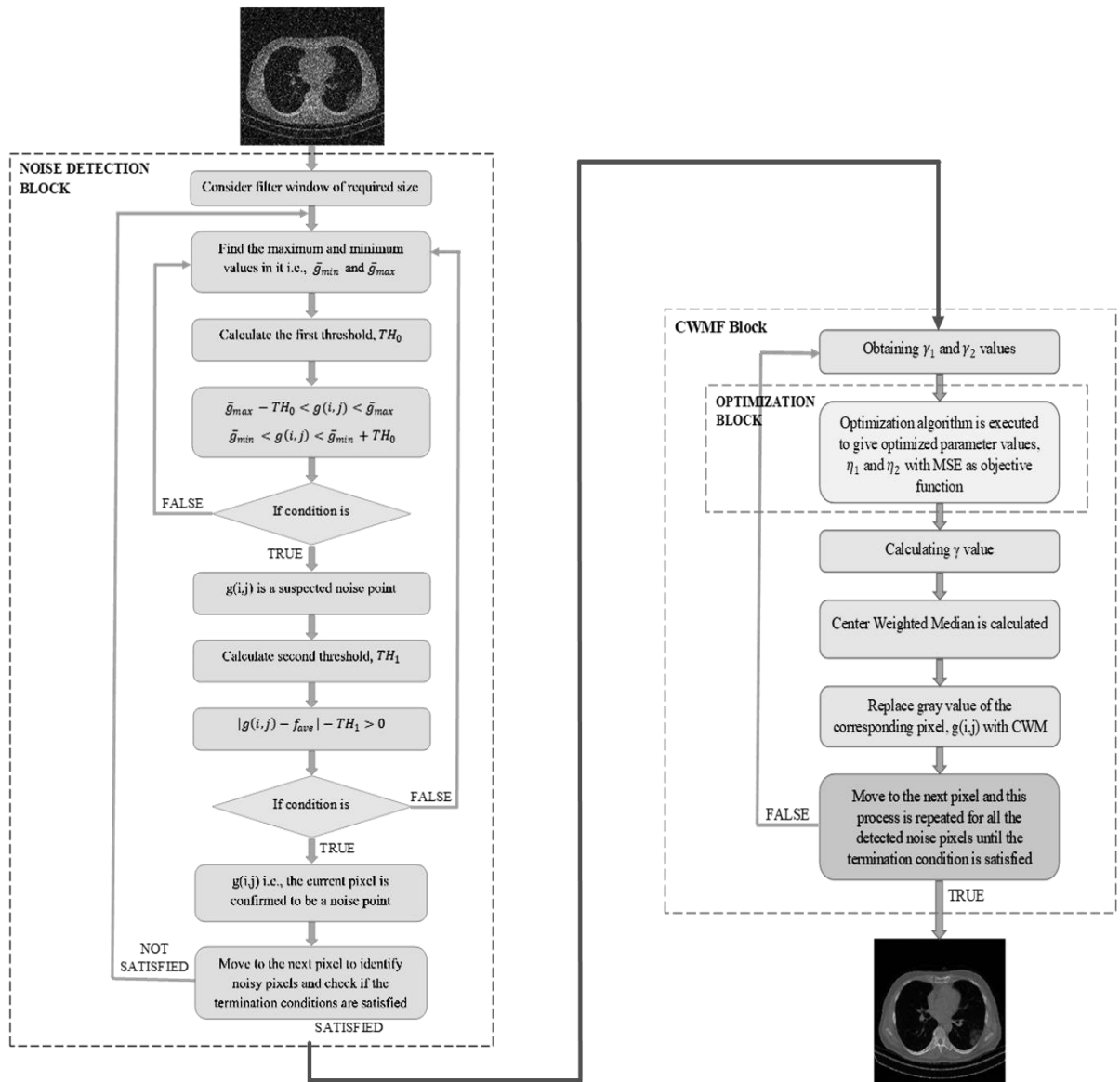


Figure 5.12 Flowchart depicting the complete process

# CHAPTER VI

## RESULTS AND DISCUSSIONS

### 6.1 Introduction

Adenovirus pneumonia introduced into (10%,20%,30%,40%,50%,60%,70%) of several COVID-19 CT picture types, including early COVID-19, advanced COVID19, early COVID-19 with no symptoms, and advanced COVID-19 with no symptoms, are evaluated for impulsive noise.

There are a number of metrics that are frequently used in image processing to assess how well the output compares to the input. Four such metrics are noise densities, mean squared error (MSE), peak signal-to-noise ratio (PSNR), image enhancement factor (IEF), weight parameters ( $\gamma_1$  and  $\gamma_2$ ).

The amount of noise in an image or signal is referred to as its noise density. It is often calculated as the difference between the variances of the noise and the signal. A lower signal-to-noise ratio, or higher noise density, makes it more difficult to separate the signal from the noise.

### 6.2 Image Quality Metrics

In addition to noise densities, MSE, PSNR, and IEF, weight parameters are also commonly used in signal processing to evaluate the quality of the output. Weight parameters refer to the coefficients used in algorithms that manipulate signals or images, such as filters or neural networks. These weight parameters are optimized during the training process to achieve the best performance.

By measuring how closely the output signal or image resembles the input signal or image, MSE and PSNR can be used to assess the output signal or image's quality. The closer the output is to the input, the lower the MSE value or higher the PSNR value.



Weight parameters can be adjusted to optimize these values and improve the overall quality of the output.

IEF, on the other hand, is used to assess how well an image's contrast has improved. This statistic can be used to assess how effectively weight factors during image processing have enhanced the contrast of an image.

In signal processing, weight parameters can be adjusted to optimize various aspects of the output signal or image. For example, in a neural network used for image classification, weight parameters can be optimized to improve accuracy. In image processing, weight parameters can be optimized to reduce noise or improve image quality.

Overall, these metrics and weight parameters are important tools in signal and image processing. It is feasible to enhance output quality and maximise algorithm performance by carefully altering weight parameters and examining the metrics that result.

### **6.2.1 PSNR**

Peak Signal-to-Noise Ratio, or PSNR, is a commonly used statistic in digital signal processing and image processing to assess how well an output signal or image compares to the source or reference signal or image. It calculates the difference between a signal or image's peak signal power and its noise power.

The PSNR is determined using the following formula and expressed in decibels (dB):

$$PSNR = 10 \times \log \left( \frac{255^2}{MSE} \right)$$

A higher PSNR value indicates that the output signal or image is closer to the original, i.e., it has lower distortion or noise. The maximum possible value of PSNR is typically 60 dB, which corresponds to a perfect reconstruction of the original signal or image.

In applications like image and video compression, where the objective is to minimise the quantity of the data while keeping an acceptable level of quality, PSNR is frequently

utilised. It is also used to assess how well different image processing techniques, like denoising, deblurring, and super-resolution, perform.

However, PSNR has some limitations as a quality metric, as it does not always correlate well with human perception of image quality. In particular, it tends to overemphasize the importance of pixel-level differences and does not take into account perceptual factors such as contrast and color. As a result, PSNR has been challenged in some applications by other metrics including the Structural Similarity Index (SSIM) and Visual Information Fidelity (VIF).

### 6.2.2 MSE

In signal and image processing, the metric known as MSE (Mean Squared Error) is frequently used to compare two signals or images. In terms of signals or images, it is the average of the squared disparities between the pixel values.

This formula determines the MSE between two signals or pictures, X and Y:

$$MSE = \frac{1}{M \times N} \sum_{i=1}^M \sum_{j=1}^N [g(i, j) - \hat{g}(i, j)]^2$$

Where, M, N is length and width of the CT image respectively.  $g(i, j)$  and  $\hat{g}(i, j)$  represent filtered (output) and noisy (input) images respectively.

By comparing the output signal or picture to the original or reference signal or image, MSE is used to assess the quality of a signal or image processing algorithm's output signal or image. A lower MSE value indicates better similarity between the two signals or images

MSE is frequently employed in applications where the objective is to decrease the quantity of the data while retaining an acceptable level of quality, such as picture and video compression. It is also used to assess how well different image processing techniques, like denoising, deblurring, and super-resolution, perform.

However, MSE has some limitations as a quality metric, as it does not always correlate well with human perception of image quality. In particular, it tends to

overemphasize the importance of pixel-level differences and does not take into account perceptual factors such as contrast and color. As a result, other metrics such as Structural Similarity Index (SSIM) and Visual Information Fidelity (VIF) have been proposed as alternatives to MSE in some applications.

### 6.2.3 IEF

An image's improvement in contrast after being processed by an image enhancement method is measured using the IEF (Image Enhancement Factor) metric in image processing. By changing the pixel values in an image, image enhancement algorithms seek to enhance the visual quality of the image. Typically, this is done by manipulating the brightness, contrast, or colour balance.

IEF is defined as the contrast ratio between the improved image and the original image. The difference between an image's maximum and least pixel values is referred to as contrast.

$$IEF = \frac{\sum_{i=1}^M \sum_{j=1}^N [I(i,j) - \hat{g}(i,j)]^2}{\sum_{i=1}^M \sum_{j=1}^N [g(i,j) - \hat{g}(i,j)]^2}$$

Where  $I(i,j)$  represent pixel values of original image.  $g(i,j)$  and  $\hat{g}(i,j)$  represent pixel values of filtered (output) and noisy image (input) respectively.

A higher IEF value indicates a greater improvement in contrast after image enhancement. IEF is used to assess the effectiveness of different image enhancement algorithms and to contrast distinct methods.

However, like other metrics used in image processing, IEF has some limitations. It only evaluates contrast improvement and does not consider other perceptual factors such as sharpness, color fidelity, and noise reduction. In order to assess image quality following image augmentation, additional metrics like the Structural Similarity Index (SSIM) and Visual Information Fidelity (VIF) are also utilised.

### 6.3 Simulated Parameter Values

Table 6.1 Weight parameters, MSE, PSNR, IEF values of different noise densities of different CT images of COVID-19 using Aquila optimizer

Image type	Noise density	$\eta_1$	$\eta_2$	MSE	PSNR	IEF
early COVID-19	10%	4.7775	7.3771	88.2219	28.675	29.9165
	20%	9.5539	4.4244	92.1088	28.4878	57.0982
	30%	5.3626	7.6741	104.3813	27.9446	75.0914
	40%	6.8945	6.3083	133.8242	26.8655	79.1676
	50%	7.3962	5.4339	173.4218	25.7398	75.5392
	60%	7.4168	8.1201	278.3672	23.6846	56.9305
	70%	7.2725	5.1714	824.7231	18.9677	22.3438
advanced COVID-19	10%	6.2287	9.4118	71.9663	29.5592	34.5259
	20%	5.7387	8.0624	76.1516	29.314	65.6819
	30%	4.5137	5.3304	91.7229	28.506	81.5941
	40%	8.1495	9.9956	116.6659	27.4614	85.7342
	50%	9.2607	9.2141	148.7574	26.406	83.7848
	60%	7.27	5.5196	236.8459	24.3861	62.926
	70%	1.3707	8.6813	1213.30	17.291	14.3456
early with non-symptom	10%	7.6026	6.7972	72.0452	29.5548	33.1349
	20%	4.7433	9.1477	82.4943	28.9666	58.6438
	30%	8.7633	8.6785	97.8776	28.224	73.5688
	40%	8.8208	9.3316	130.6732	26.9689	73.7124
	50%	3.2737	9.5879	172.7378	25.7569	69.819
	60%	8.8664	4.886	292.1739	23.4744	49.5672
	70%	8.7456	1.2845	1112.20	17.669	15.1752
advanced with non-symptom	10%	8.9785	8.3484	36.2991	32.5318	67.4777
	20%	7.3535	8.0441	38.7479	32.2483	127.8829
	30%	6.1748	5.2665	50.4984	31.0981	148.0584
	40%	7.2889	9.5617	83.2912	28.9248	119.5978
	50%	8.1847	2.8521	133.7774	26.867	92.3058
	60%	7.8845	8.7627	261.7173	23.9525	57.0147
	70%	3.5334	3.5162	1011.90	18.0792	17.1311
adenovirus pneumonia	10%	5.75	9.0417	144.6921	26.5264	17.0535
	20%	8.7894	7.1022	167.7017	25.8854	29.6472
	30%	9.9385	8.9314	211.4781	24.8782	35.0874
	40%	7.8673	8.1714	298.4103	23.3827	33.1606
	50%	5.4037	7.3896	487.6168	21.25	25.21
	60%	7.3534	8.143	637.8083	20.0839	23.3328
	70%	2.1429	5.9219	1232.80	17.2218	14.088

**Table 6.2** Weight parameters, PSNR, IEF values of different noise densities of different CT images of COVID-19 using Arithmetic optimization algorithm

<b>Image type</b>	<b>Noise density</b>	$\eta_1$	$\eta_2$	<b>MSE</b>	<b>PSNR</b>	<b>IEF</b>
<b>early COVID-19</b>	10%	8.6783	9.8838	86.9201	28.7396	30.5172
	20%	9.9836	7.8807	88.4566	28.6635	59.5123
	30%	8.817	7.726	99.3378	28.1597	79.0875
	40%	4.7047	7.5587	130.533	26.9736	80.7202
	50%	5.3139	8.9525	169.8837	25.8293	77.1206
	60%	9.5354	7.853	258.8164	24.0009	61.1236
	70%	8.5709	4.3161	823.5948	18.9737	22.3763
<b>advanced COVID-19</b>	10%	7.5886	7.2789	67.8645	29.8144	36.6814
	20%	6.3269	8.6104	76.2822	29.3066	65.0123
	30%	7.1054	8.2487	85.7012	28.8009	87.5801
	40%	7.8021	7.0099	116.58	27.4646	85.5207
	50%	6.2015	9.7826	156.7998	26.1773	79.6337
	60%	9.2204	9.6176	217.0931	24.7643	68.5537
	70%	3.0608	9.9652	773.4155	19.2467	22.4875
<b>early with non-symptom</b>	10%	6.836	7.2955	74.6458	29.4007	32.2985
	20%	6.1244	6.0157	84.8471	28.8444	56.2925
	30%	9.1707	8.2281	94.9335	28.3566	75.486
	40%	5.4441	9.5833	126.2051	27.12	76.2969
	50%	9.2253	6.2221	165.2708	25.9488	72.8295
	60%	6.8111	7.1327	275.9737	23.7222	52.3348
	70%	5.6516	3.6848	880.5535	18.6832	19.1137
<b>advanced with non-symptom</b>	10%	7.8792	9.2274	36.3965	32.5202	68.4631
	20%	5.6854	8.9376	37.687	32.3689	131.9816
	30%	8.9578	4.5448	51.3302	31.0271	145.1484
	40%	7.6296	9.5332	78.6199	29.1755	126.525
	50%	2.9279	9.1713	125.6892	27.1378	98.1727
	60%	8.2308	6.0992	246.0799	24.22	60.0383
	70%	7.9686	3.0316	829.1055	18.9447	20.913
<b>adenovirus pneumonia</b>	10%	7.7614	9.6336	142.6033	26.5895	17.1896
	20%	8.3907	7.5855	163.8246	25.9871	30.2431
	30%	7.6967	6.559	216.9422	24.7674	34.3776
	40%	8.9169	4.8273	303.3671	23.3111	32.6104
	50%	5.8667	9.4585	470.2793	21.4072	26.4203
	60%	8.7889	8.2121	634.5647	20.1066	23.4857
	70%	1.5103	9.1464	1140.9077	17.5583	15.1599

## 6.4 Resultant CT Images

### 6.4.1 Filtered Images using Aquila optimizer

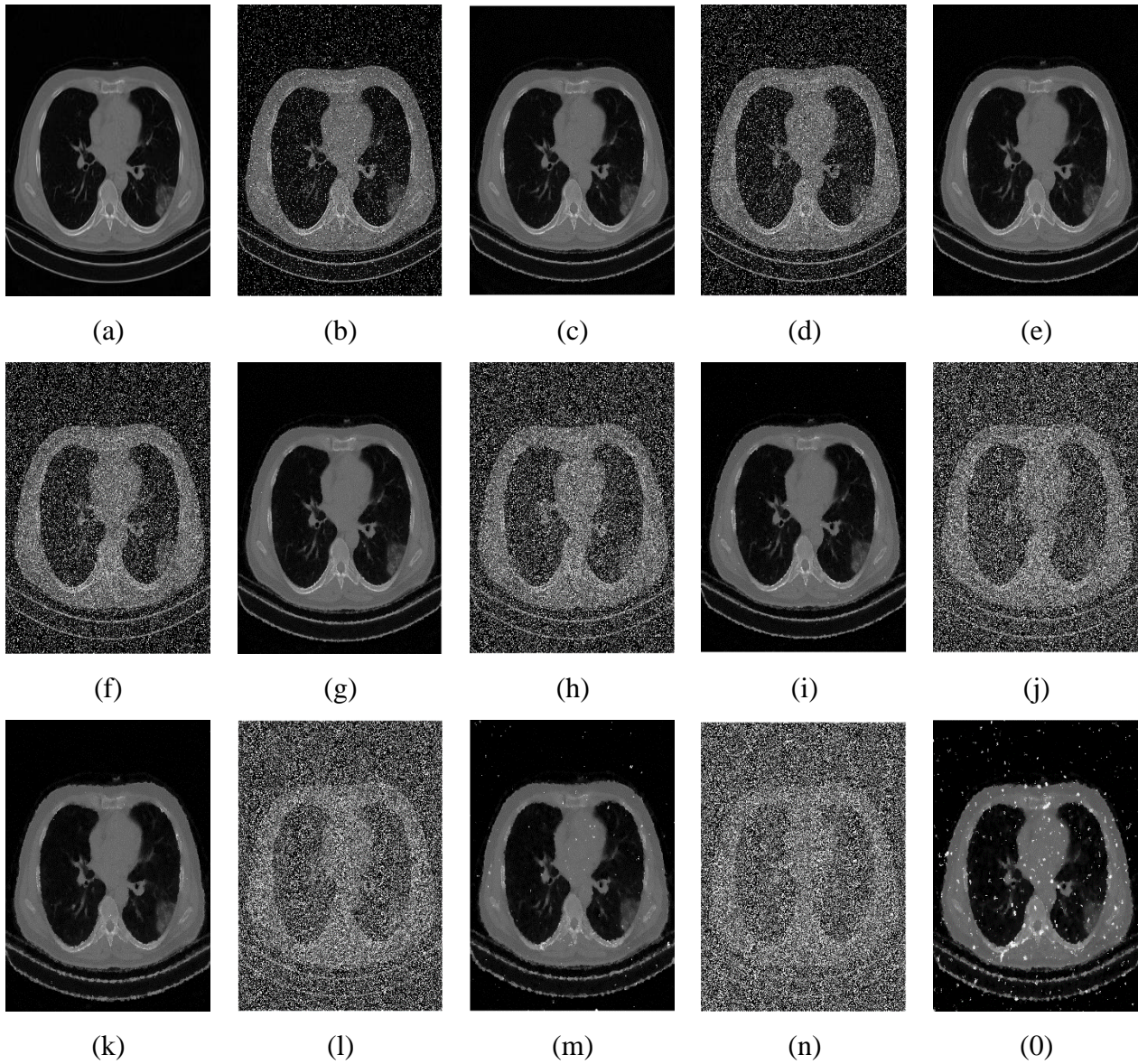


Figure 6.1 CT image of early COVID -19 (a) original image; (b) impulse (10%) noise; (c) filtered image of (b); (d) impulse (20%) noise; (e) filtered image of (d); (f) impulse (30%) noise; (g) filtered image of (f); (h) impulse (40%) noise; (i) filtered image of (h); (j) impulse (50%) noise; (k) filtered image of (j); (l) impulse (60%) noise; (m) filtered image of (l); (n) impulse (70%) noise; (o) filtered image of (n)



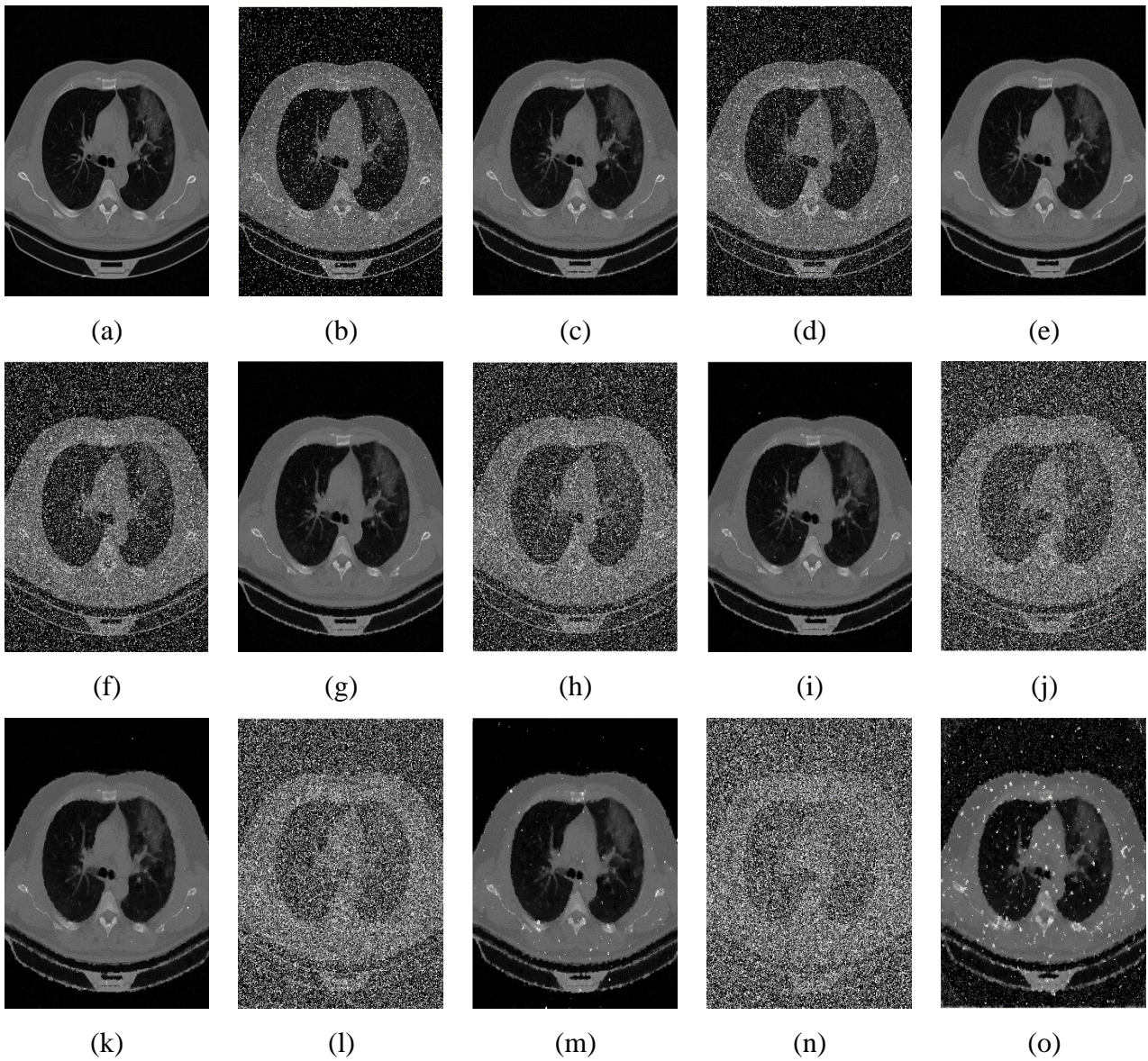


Figure 6.2 CT image of advanced COVID -19 (a) original image; (b) impulse (10%) noise; (c) filtered image of (b); (d) impulse (20%) noise; (e) filtered image of (d); (f) impulse (30%) noise; (g) filtered image of (f); (h) impulse (40%) noise; (i) filtered image of (h); (j) impulse (50%) noise; (k) filtered image of (j); (l) impulse (60%) noise; (m) filtered image of (l); (n) impulse (70%) noise; (o) filtered image of (n)



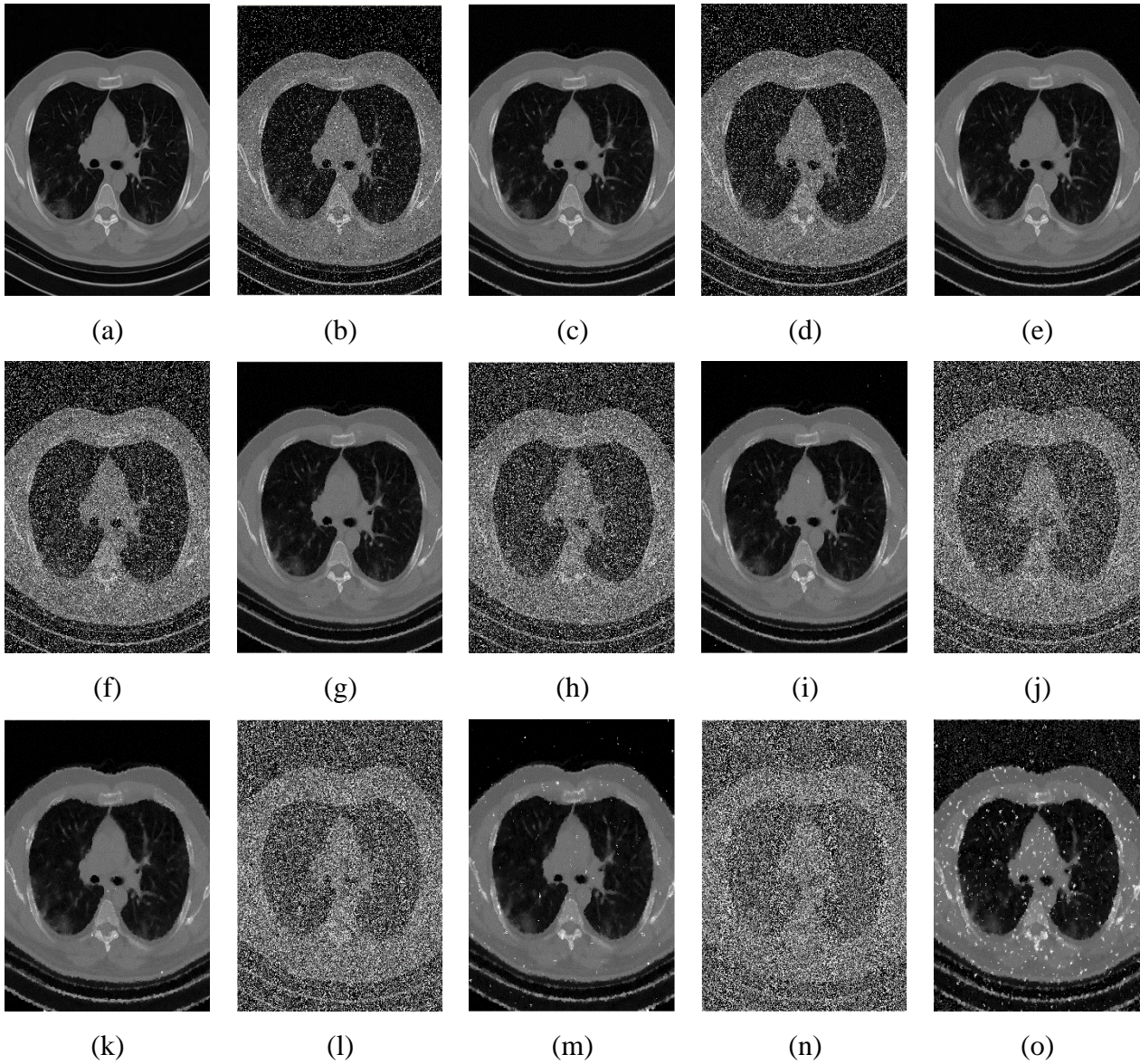


Figure 6.3 CT image of early COVID -19 with non-symptom (a) original image; (b) impulse (10%) noise; (c) filtered image of (b); (d) impulse (20%) noise; (e) filtered image of (d); (f) impulse (30%) noise; (g) filtered image of (f); (h) impulse (40%) noise; (i) filtered image of (h); (j) impulse (50%) noise; (k) filtered image of (j); (l) impulse (60%) noise; (m) filtered image of (l); (n) impulse (70%) noise; (o) filtered image of (n)



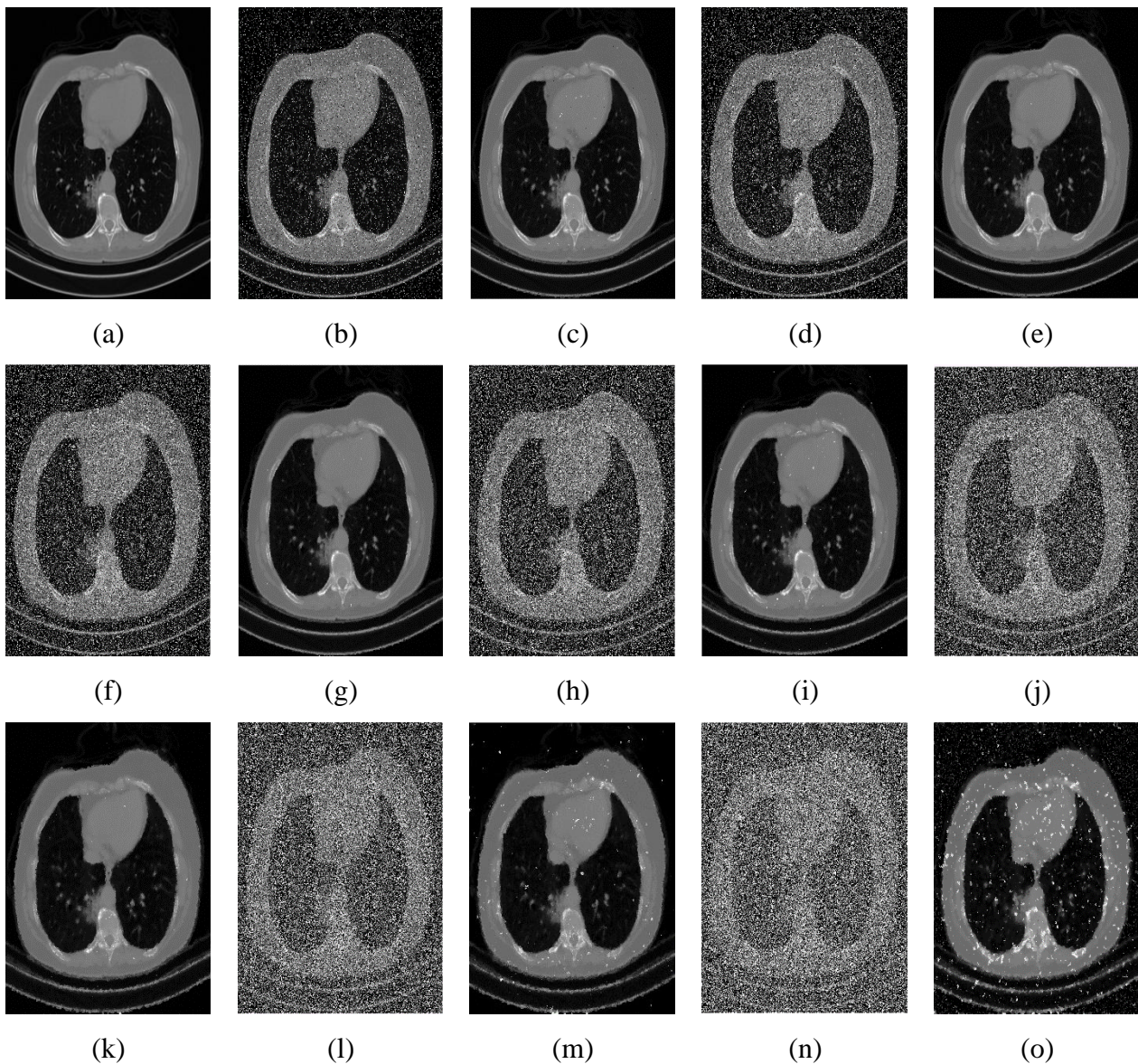


Figure 6.4 CT image of advanced COVID -19 with non-symptom (a) original image; (b) impulse (10%) noise; (c) filtered image of (b); (d) impulse (20%) noise; (e) filtered image of (d); (f) impulse (30%) noise; (g) filtered image of (f); (h) impulse (40%) noise; (i) filtered image of (h); (j) impulse (50%) noise; (k) filtered image of (j); (l) impulse (60%) noise; (m) filtered image of (l); (n) impulse (70%) noise; (o) filtered image of (n)



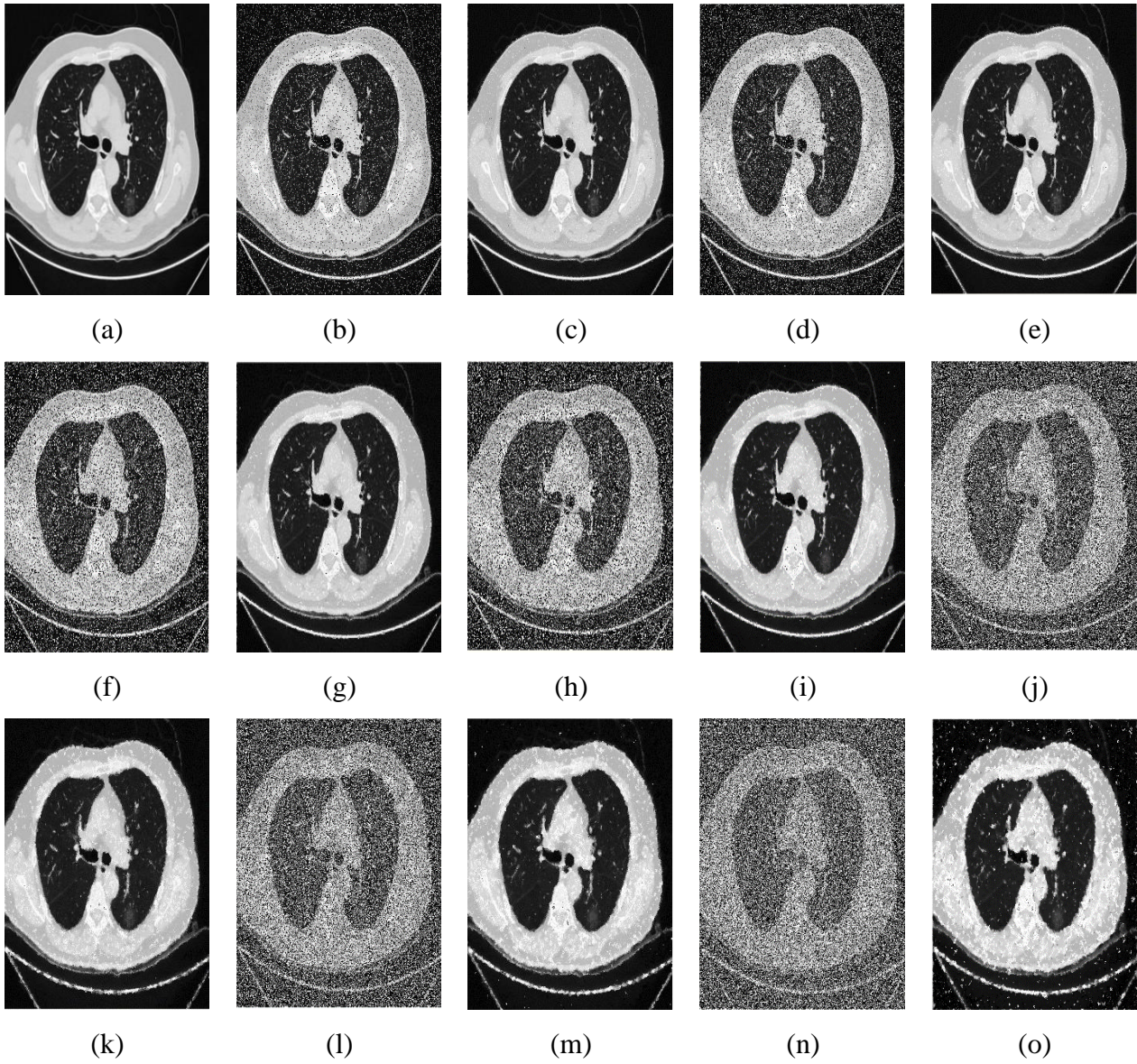


Figure 6.5 CT image of adenovirus pneumonia (suspected cases of COVID-19) (a) original image; (b) impulse (10%) noise; (c) filtered image of (b); (d) impulse (20%) noise; (e) filtered image of (d); (f) impulse (30%) noise; (g) filtered image of (f); (h) impulse (40%) noise; (i) filtered image of (h); (j) impulse (50%) noise; (k) filtered image of (j); (l) impulse (60%) noise; (m) filtered image of (l); (n) impulse (70%) noise; (o) filtered image of (n)



### 6.4.2 Filtered Images using Arithmetic optimizer

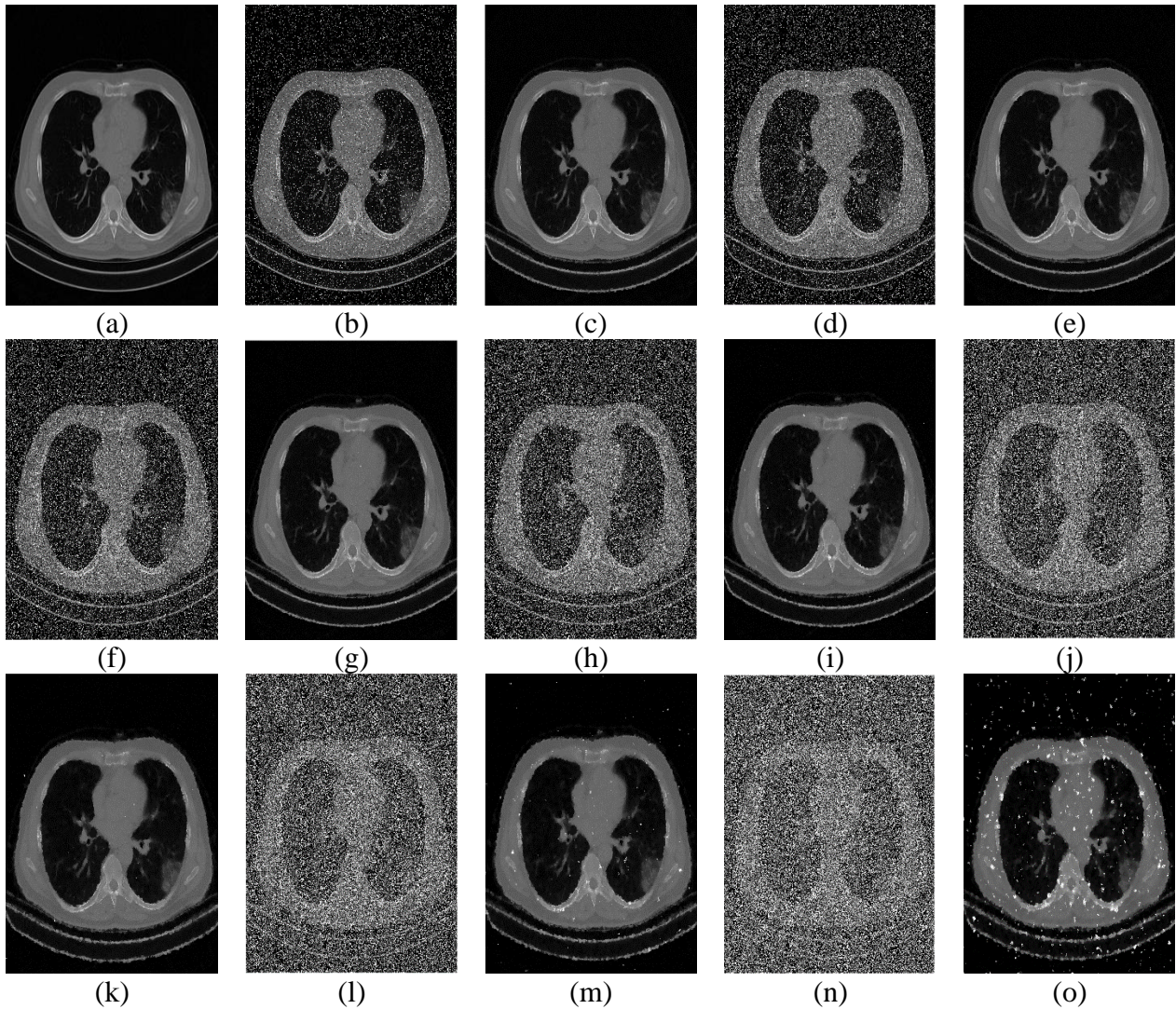


Figure 6.6 CT image of early COVID -19 (a) original image; (b) impulse (10%) noise; (c) filtered image of (b); (d) impulse (20%) noise; (e) filtered image of (d); (f) impulse (30%) noise; (g) filtered image of (f); (h) impulse (40%) noise; (i) filtered image of (h); (j) impulse (50%) noise; (k) filtered image of (j); (l) impulse (60%) noise; (m) filtered image of (l); (n) impulse (70%) noise; (o) filtered image of (n)



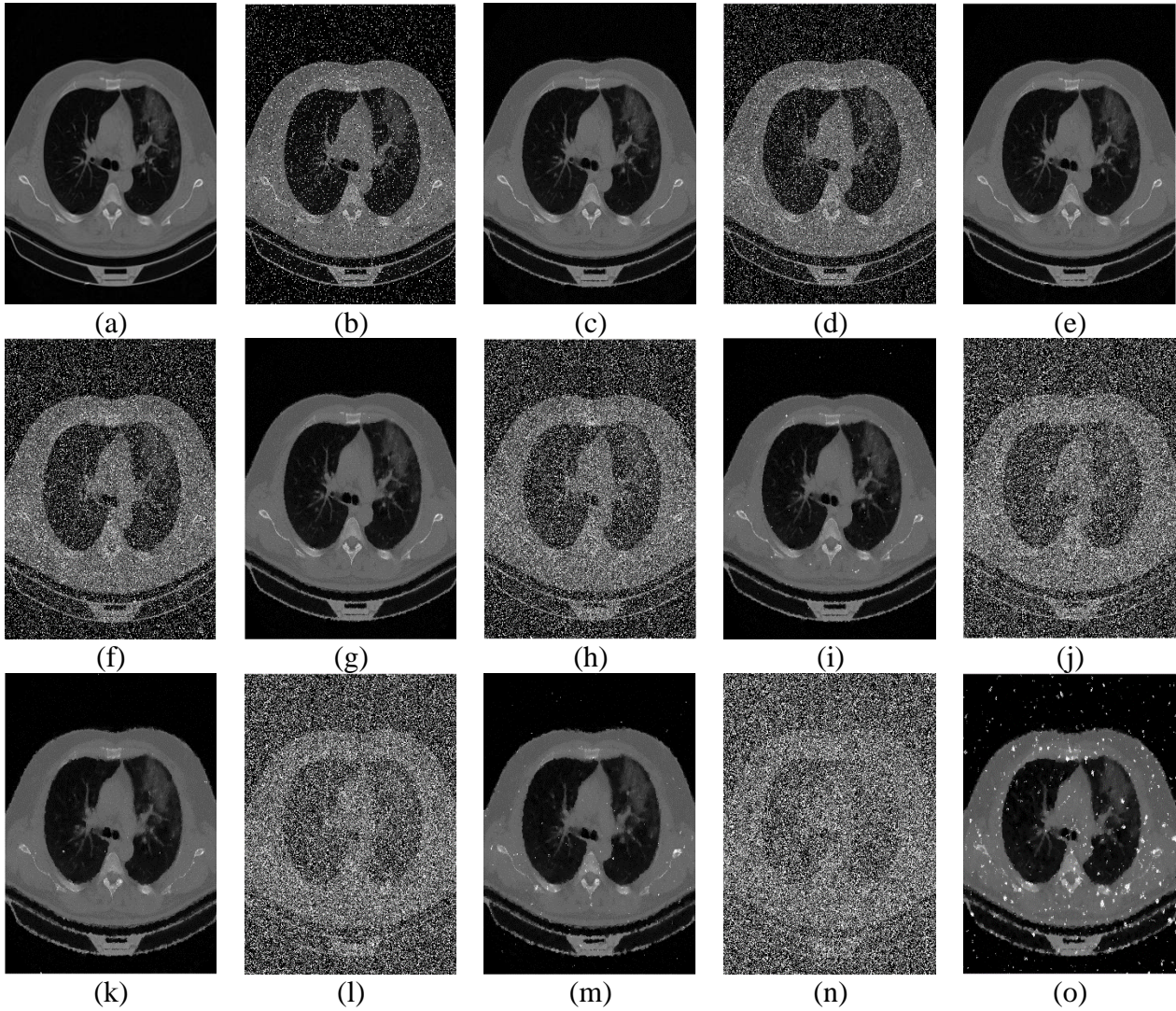


Figure 6.7 CT image of advanced COVID -19 (a) original image; (b) impulse (10%) noise; (c) filtered image of (b); (d) impulse (20%) noise; (e) filtered image of (d); (f) impulse (30%) noise; (g) filtered image of (f); (h) impulse (40%) noise; (i) filtered image of (h); (j) impulse (50%) noise; (k) filtered image of (j); (l) impulse (60%) noise; (m) filtered image of (l); (n) impulse (70%) noise; (o) filtered image of (n)



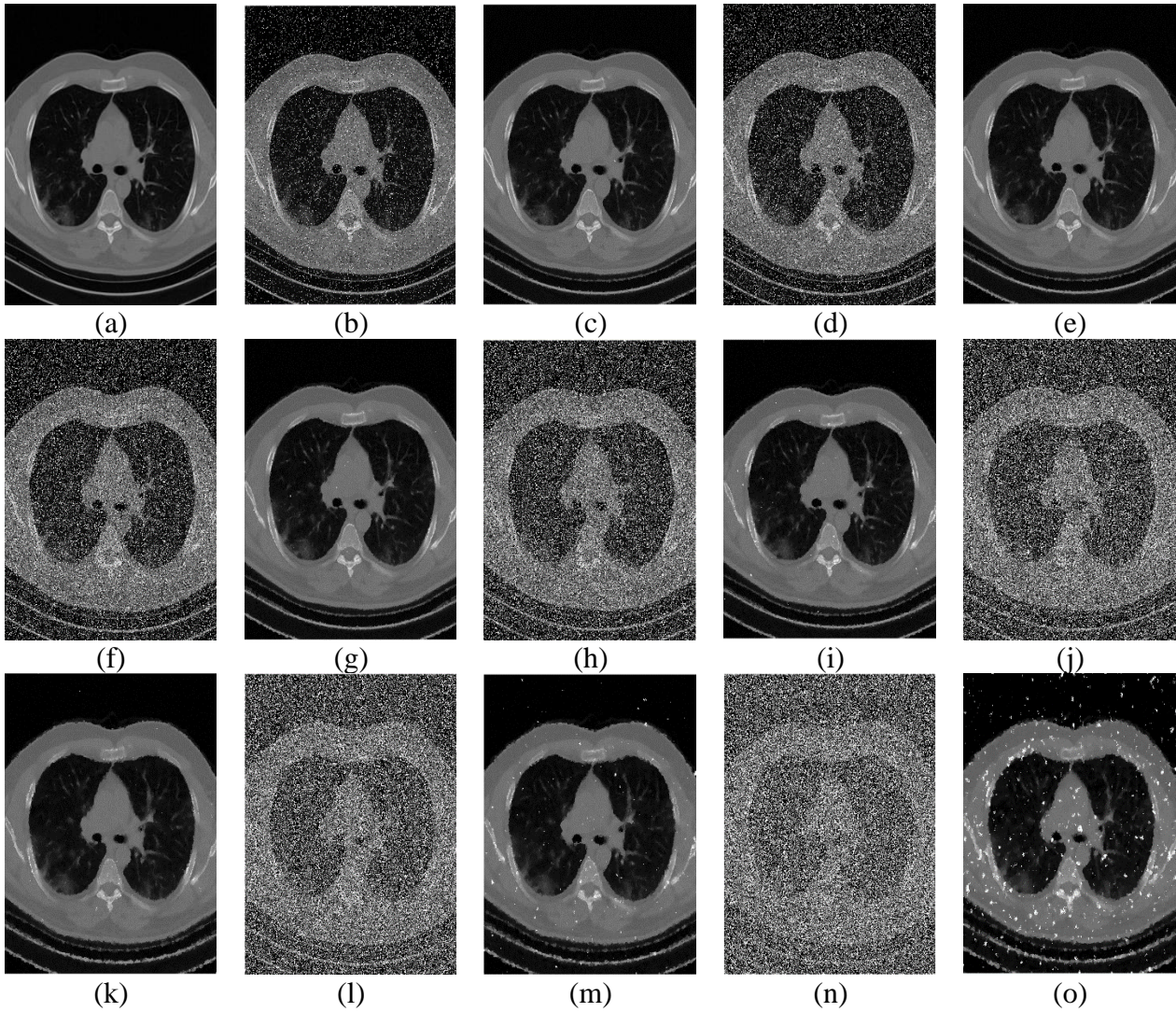


Figure 6.8 CT image of early COVID -19 with non-symptom (a) original image; (b) impulse (10%) noise; (c) filtered image of (b); (d) impulse (20%) noise; (e) filtered image of (d); (f) impulse (30%) noise; (g) filtered image of (f); (h) impulse (40%) noise; (i) filtered image of (h); (j) impulse (50%) noise; (k) filtered image of (j); (l) impulse (60%) noise; (m) filtered image of (l); (n) impulse (70%) noise; (o) filtered image of (n)



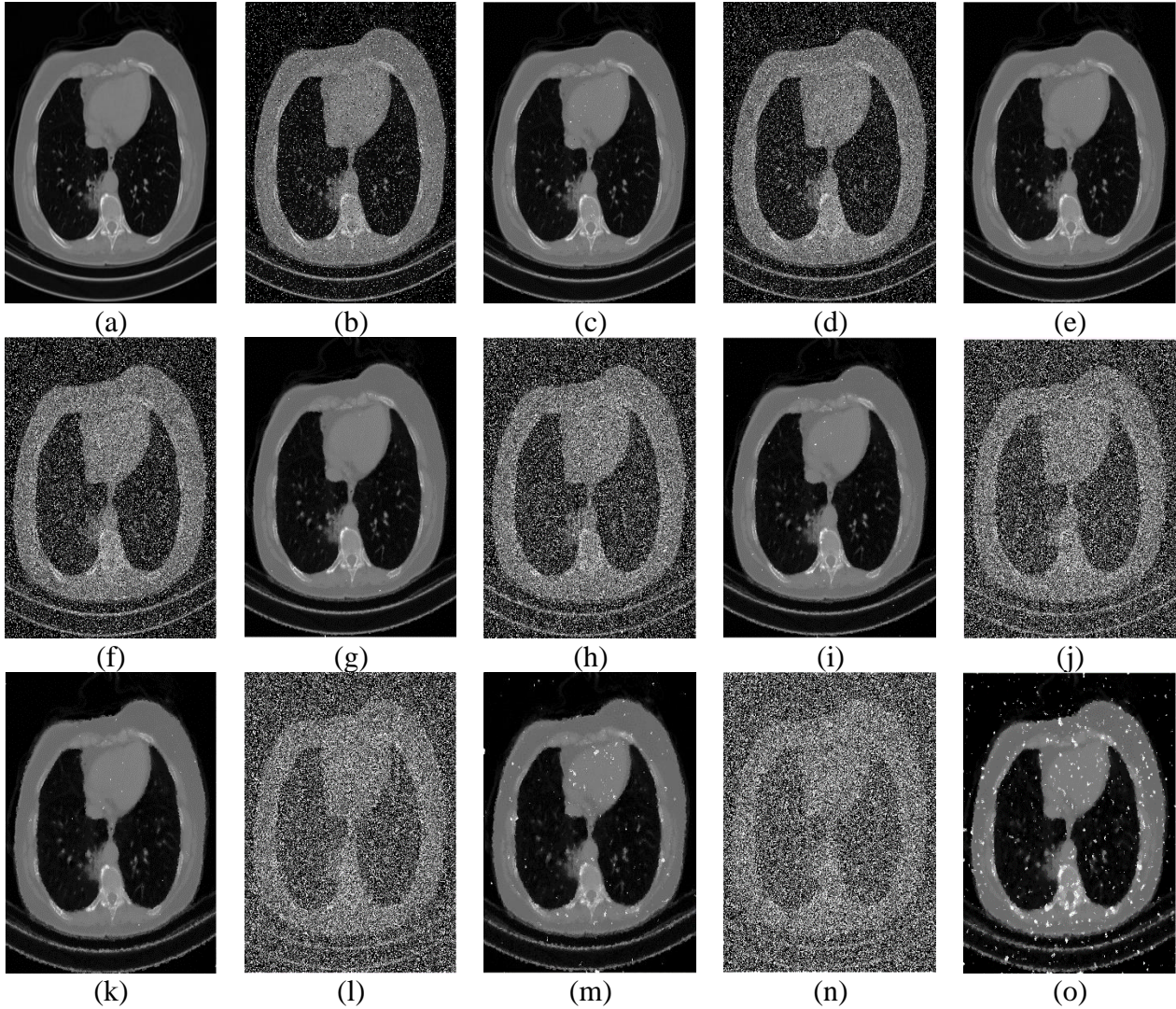


Figure 6.9 CT image of advanced COVID -19 with non-symptom (a) original image; (b) impulse (10%) noise; (c) filtered image of (b); (d) impulse (20%) noise; (e) filtered image of (d); (f) impulse (30%) noise; (g) filtered image of (f); (h) impulse (40%) noise; (i) filtered image of (h); (j) impulse (50%) noise; (k) filtered image of (j); (l) impulse (60%) noise; (m) filtered image of (l); (n) impulse (70%) noise; (o) filtered image of (n)



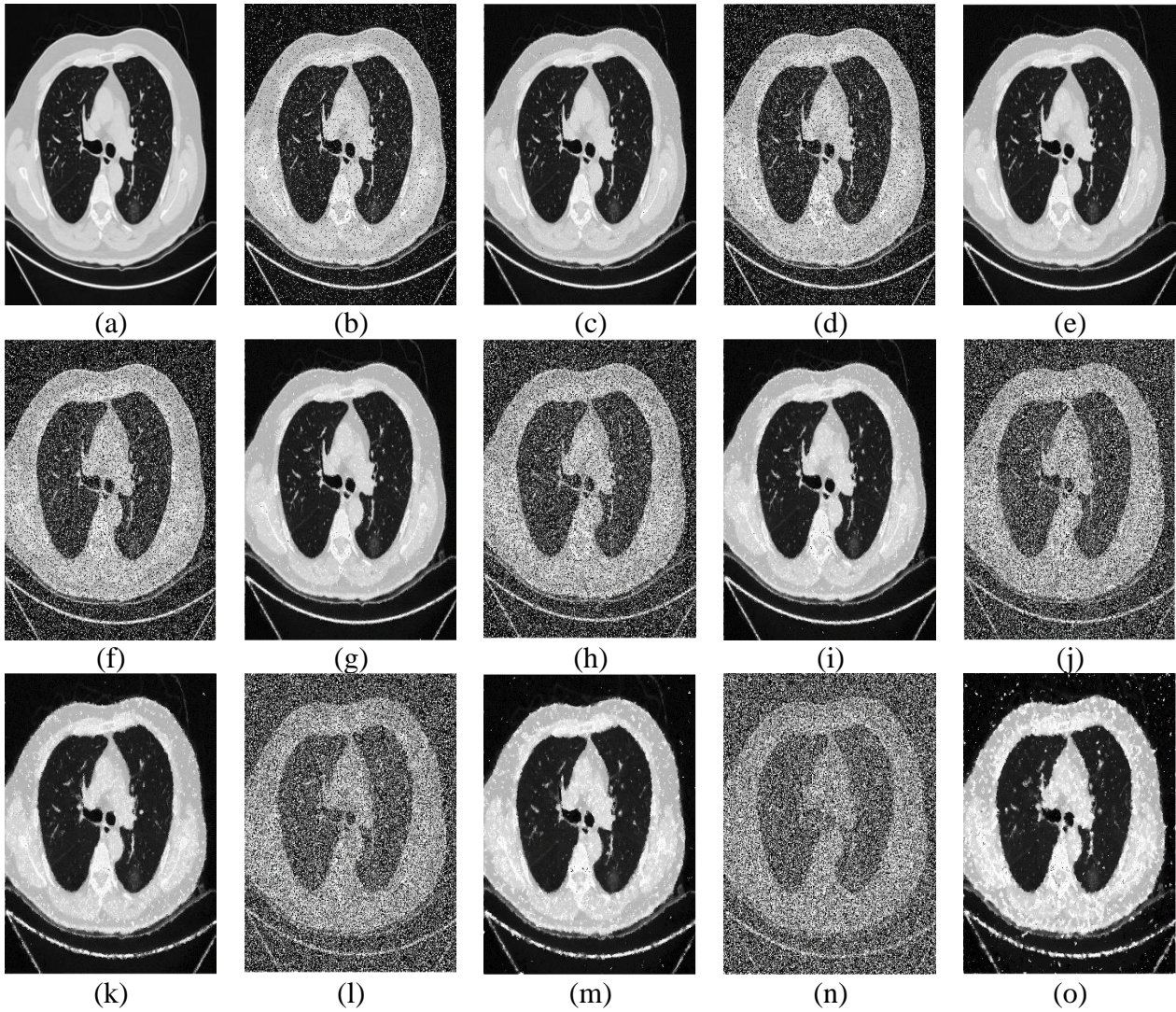
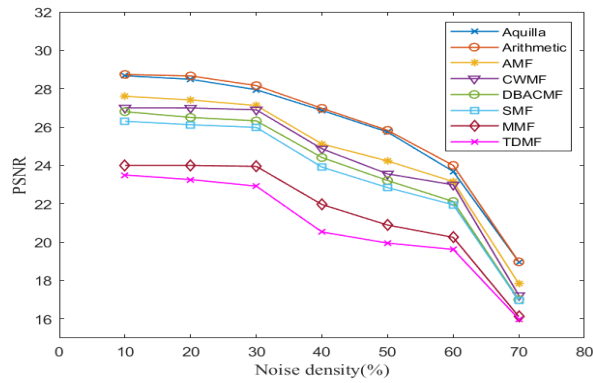
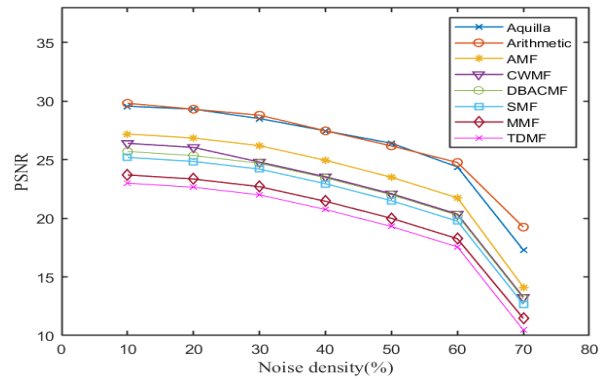


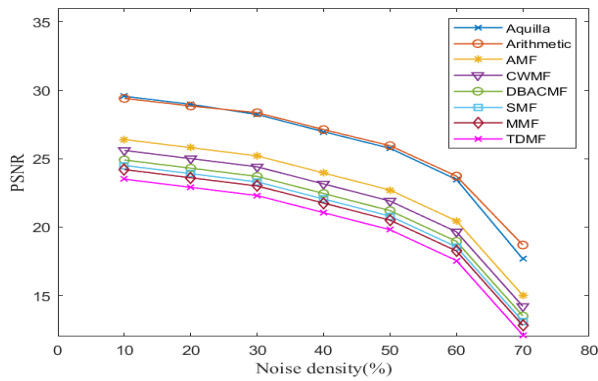
Figure 6.10 CT image of adenovirus pneumonia (suspected cases of COVID-19) (a) original image; (b) impulse (10%) noise; (c) filtered image of (b); (d) impulse (20%) noise; (e) filtered image of (d); (f) impulse (30%) noise; (g) filtered image of (f); (h) impulse (40%) noise; (i) filtered image of (h); (j) impulse (50%) noise; (k) filtered image of (j); (l) impulse (60%) noise; (m) filtered image of (l); (n) impulse (70%) noise; (o) filtered image of (n)



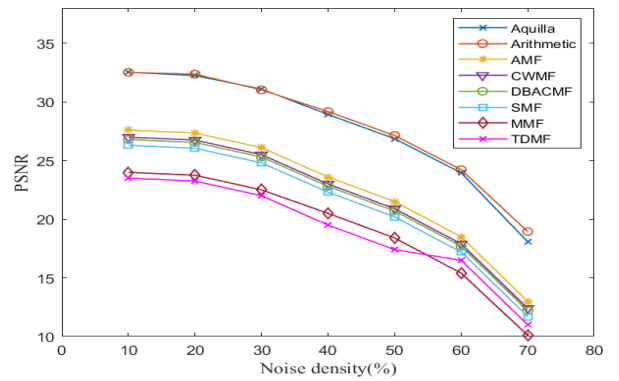
(a)



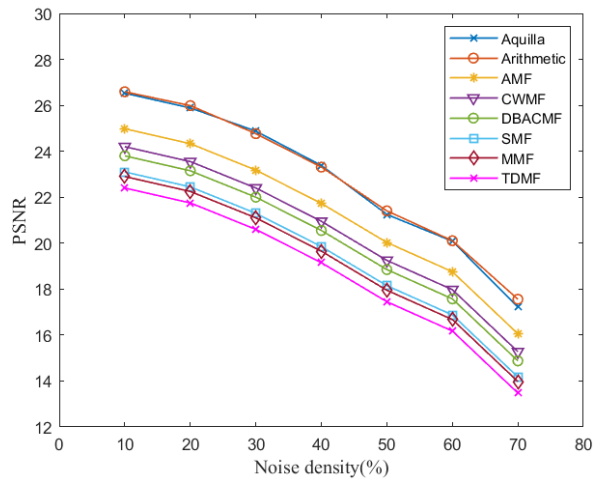
(b)



(c)



(d)



(e)

Figure 6.11 Comparison of PSNR for CT scans with varying noise densities for: (a) Early COVID-19, (b) advanced COVID-19, (c) Early COVID-19 with non-symptom, (d) Advanced COVID-19 with non-symptom, (e) Adenovirus pneumonia; for different filtering techniques.



## 6.4 Result Analysis

Table 6.1 and 6.2 compares the considered metrics along with optimization parameters for the considered AO and AOA techniques for different stages of COVID-19 CT scans with varying noise densities (10% to 70%). Figures (6.1-6.10) shows CT images of various phases of COVID-19 representing the actual and filtered images of respective images with varying noise densities.

Fig. 6.11 gives out the comparison of PSNR values for different methods. It can be interpreted that AO and AOA techniques exhibit desired high PSNR values compared to other methods. This suggests that the filtered image that was obtained is fairly close to the original image.

Thus, it can be concluded through the results that optimized parameter values,  $\eta_1$  and  $\eta_2$  gave better PSNR (high) and MSE (low) values compared to other traditional filters.

## **CHAPTER VII**

### **CONCLUSION AND FUTURE WORK**

In this project, a CT scan denoising approach using multi-level thresholding combined with optimized center weighted median filter has been proposed and tested. With thresholding approach being adaptive in nature, ensures proper detection of noise points with less error probability. In this project filter window of different size ( $5 \times 5$  and  $7 \times 7$ ) have been considered based on the noise density of the image. For larger noise densities ( $>50\%$ ) filter window of size  $7 \times 7$  has been considered and for the other low noise densities a  $5 \times 5$  window is considered. The change in window size is attributed to the noise density, as a bigger window size implies availability of more non-noisy pixels. This makes it suitable for better estimation of center pixel value that is to be replaced with corresponding noisy pixel. Lastly, the CWM filter used with optimization block ensures our objective of replacing the noise points with better values ultimately to achieve a proper denoised image.

As for the future developments is concerned, the denoising approach proposed here is with respect to a CT scan. In the same way a denoising approach for MRI scan can be found considering respective MRI scan parameters which differ from that of CT. Another possibility could be regarding the type of noise focused on. This project is concerned with removal of salt and pepper noise (impulse noise) and the same could be applied for other types of noise existing like Gaussian noise, mixed noise which affect the CT image just like the impulse noise does.

## REFERENCES

- [1] C. Lin et al., “Comparison of throat swabs and sputum specimens for viral nucleic acid detection in 52 cases of novel coronavirus (SARS-Cov-2)-infected pneumonia (COVID-19),” *Clin Chem Lab Med*, vol. 58, no. 7, pp. 1089–1094, Jul. 2020, doi: 10.1515/cclm-2020-0187.
- [2] Y. Li *et al.*, “Stability issues of RT-PCR testing of SARS-CoV-2 for hospitalized patients clinically diagnosed with COVID-19,” *J Med Virol*, vol. 92, no. 7, pp. 903–908, Jul. 2020, doi: 10.1002/jmv.25786.
- [3] A. Tahamtan and A. Ardebili, “Real-time RT-PCR in COVID-19 detection: issues affecting the results,” *Expert Review of Molecular Diagnostics*, vol. 20, no. 5. Taylor and Francis Ltd, pp. 453–454, May 03, 2020. doi: 10.1080/14737159.2020.1757437
- [4] T. Ai *et al.*, “Correlation of Chest CT and RT-PCR Testing in Coronavirus Disease 2019 (COVID-19) in China: A Report of 1014 Cases.”
- [5] A. Bernheim *et al.*, “Duration of Infection.”
- [6] W. Xia, J. Shao, Y. Guo, X. Peng, Z. Li, and D. Hu, “Clinical and CT features in pediatric patients with COVID-19 infection: Different points from adults,” *Pediatr Pulmonol*, vol. 55, no. 5, pp. 1169–1174, May 2020, doi: 10.1002/ppul.24718.
- [7] M. Carotti et al., “Chest CT features of coronavirus disease 2019 (COVID-19) pneumonia: key points for radiologists,” *Radiologia Medica*, vol. 125, no. 7. Springer, pp. 636–646, Jul. 01, 2020. doi: 10.1007/s11547-020-01237-4.

- [8] J. Azadbakht et al., “A review on chest CT scanning parameters implemented in COVID-19 patients: bringing low-dose CT protocols into play,” *Egyptian Journal of Radiology and Nuclear Medicine*, vol. 52, no. 1. Springer Science and Business Media Deutschland GmbH, Dec. 01, 2021. doi: 10.1186/s43055-020-00400-1.
- [9] S. Guo, G. Wang, L. Han, X. Song, and W. Yang, “COVID-19 CT image denoising algorithm based on adaptive threshold and optimized weighted median filter,” *Biomed Signal Process Control*, vol. 75, May 2022, doi: 10.1016/j.bspc.2022.103552.
- [10] L. Abualigah, D. Yousri, M. Abd Elaziz, A. A. Ewees, M. A. A. Al-qaness, and A. H. Gandomi, “Aquila Optimizer: A novel meta-heuristic optimization algorithm,” *Comput Ind Eng*, vol. 157, Jul. 2021, doi: 10.1016/j.cie.2021.107250.
- [11] L. Abualigah, A. Diabat, S. Mirjalili, M. Abd Elaziz, and A. H. Gandomi, “The Arithmetic Optimization Algorithm,” *Comput Methods Appl Mech Eng*, vol. 376, Apr. 2021, doi: 10.1016/j.cma.2020.113609.
- [12] A. Shah et al., “Comparative analysis of median filter and its variants for removal of impulse noise from gray scale images,” *Journal of King Saud University - Computer and Information Sciences*, vol. 34, no. 3. King Saud bin Abdulaziz University, pp. 505–519, Mar. 01, 2022. doi: 10.1016/j.jksuci.2020.03.007.
- [13] T. Tasdizen, “Principal components for non-local means image denoising,” in *Proceedings - International Conference on Image Processing, ICIP*, 2008, pp. 1728–1731. doi: 10.1109/ICIP.2008.4712108.
- [14] Z. Li, G. Liu, Y. Xu, and Y. Cheng, “Modified directional weighted filter for removal of salt & pepper noise,” *Pattern Recognit Lett*, vol. 40, no. 1, pp. 113–120, Apr. 2014, doi: 10.1016/j.patrec.2013.12.022.
- [15] Y. Lee, “Performance evaluation of noise reduction algorithm with median filter using improved thresholding method in pixelated semiconductor gamma camera system: A numerical simulation study,” *Nuclear Engineering and*

- Technology, vol. 51, no. 2, pp. 439–443, Apr. 2019, doi: 10.1016/j.net.2018.10.005.
- [16] M. Nasri, S. Saryazdi, and H. Nezamabadi-Pour, “SNLM: A switching non-local means filter for removal of high-density salt and pepper noise,” *Scientia Iranica*, vol. 20, no. 3, pp. 760–764, 2013, doi: 10.1016/j.scient.2013.01.001.
- [17] Paiva, O., 2020. CORONACASES.ORG - Helping Radiologists to Help People in More Than 100 Countries! | Coronavirus Cases - 冠状病毒病例. [online] Coronacases.org. Available at: <link> [Accessed 20 March 2020].
- [18] Glick, Y., 2020. Viewing Playlist: COVID-19 Pneumonia | Radiopaedia.Org. [online] Radiopaedia.org. Available at: <link> [Accessed 20 April 2020].
- [19] <https://coronacases.org/forum/coronacases-org-helping-radiologists-to-help-people-in-more-than-100-countries-1>
- [20] <https://zenodo.org/record/3757476#.Y9C4DKRX4zQ>
- [21] Kaggle- <https://www.kaggle.com/datasets/andrewmvd/covid19-ct-scans?resource=download>
- [22] <https://physionet.org/content/ct-ich/1.0.0/>
- [23] <https://www.kaggle.com/datasets/darren2020/ct-to-mri-cgan>

**PUBLISHED PAPER:** Communicated to Journal (ICTACT).